Pontifícia Universidade Católica
do Rio de Janeiro

Antonio Lívio de Sousa Cruz

Investigating quantum geometry and quantum criticality by a fidelity marker

Dissertação de Mestrado

Dissertation presented to the Programa de Pós–graduação em Física of PUC-Rio in partial fulfillment of the requirements for the degree of Mestre em Física.

Advisor: Prof. Wei Chen

Rio de Janeiro
August 2023

Pontifícia Universidade Católica
do Rio de Janeiro

Antonio Lívio de Sousa Cruz

Investigating quantum geometry and quantum criticality by a fidelity marker

Dissertation presented to the Programa de Pós–graduação em Física of PUC-Rio in partial fulfillment of the requirements for the degree of Mestre em Física. Approved by the Examination Committee:

Prof. Wei Chen
Advisor
Departamento de Física – PUC-Rio

Prof. Gero Arthur Hubertus Thilo Freiherr von Gersdorff
Departamento de Física – PUC-Rio

Prof. Raimundo Rocha dos Santos
UFRJ

Rio de Janeiro, August 18th, 2023

Antonio Lívio de Sousa Cruz

The author graduated in Physics from Universidade Federal do Piauí in 2021.

Bibliographic data

de Sousa Cruz, Antonio Lívio

Investigating quantum geometry and quantum criticality by a fidelity marker / Antonio Lívio de Sousa Cruz; advisor: Wei Chen. – Rio de Janeiro: PUC-Rio, Departamento de Física, 2023.

49 f: il. color. ; 30 cm

Dissertação (mestrado) - Pontifícia Universidade Católica do Rio de Janeiro, Departamento de Física, 2023.

Inclui bibliografia

1. Física – Teses. 2. Isolantes topológicos. 3. Absorção óptica. 4. Geometria quântica. 5. Transições de fase quânticas. 6. Transições de fase topológicas. I. Chen, Wei. II. Pontifícia Universidade Católica do Rio de Janeiro. Departamento de Física. III. Título.

CDD: 004

I dadicate this to my parents, friends and family
who believed in me and offered their support.

Acknowledgments

First, I want to express my eternal gratitude to my parents, Carmem Francisca de Sousa Cruz and Antonio Alves da Cruz, who are and have always been my foundation. Your efforts made by my education and training as a human being are and will be one of my biggest reasons to keep going. I also thank my aunt Meirilane Morais and her family for all the attention and support offered.

I want to thank my advisor, Prof. Wei Chen, for all your dedication in guiding me and getting me involved in our research group's projects. I want to thank you so much for your patience, even when it was hard to be. I also thank the members of our research group for all the discussions that helped me so much to grow scientifically.

To my dear friends who live with me, and who have been an excellent support network for me throughout this period. To my friends that I met at PUC-Rio and became good companions, and to my friends from Teresina, who are also practically part of my family

I wish to express my gratitude to all those who have offered their support in various forms, whether it be moral support, insightful discussions, or proofreading assistance. Your contributions have made this dissertation more robust and comprehensive.

Furthermore, I extend my appreciation to the staff and resources of the PUC-Rio, whose extensive collection of materials and efficient services have been invaluable in conducting thorough research.

This study was financed in part by the Coordenação de Aperfeiçoamento de Pessoal de Nível Superior - Brasil (CAPES) - Finance Code 001.

Abstract

de Sousa Cruz, Antonio Lívio; Chen, Wei (Advisor). **Investigating quantum geometry and quantum criticality by a fidelity marker**. Rio de Janeiro, 2023. 49p. Dissertação de Mestrado – Departamento de Física, Pontifícia Universidade Católica do Rio de Janeiro.

The investigation of quantum geometry in semiconductors and insulators has become significant due to its implications for material characteristics. The notion of quantum geometry arises by considering the quantum metric of the valence-band Bloch state, which is defined from the overlap of the Bloch states at slightly different momenta. By integrating the quantum metric throughout the Brillouin zone, we introduce a quantity that we call fidelity number, which signifies the average distance between adjacent Bloch states. Furthermore, we present a formalism to express the fidelity number as a local fidelity marker in real space that can be defined on every lattice site. The marker can be calculated directly by diagonalizing the lattice Hamiltonian that describes particle behavior on the lattice. Subsequently, the concept of the fidelity number and marker is extended to finite temperature using linear-response theory, connecting them to experimental measurements which involves analyze the global and local optical absorption power when the material is exposed to linearly polarized light. Particularly for two-dimensional materials, the material's opacity enables straightforward determination of the fidelity number spectral, allowing for experimental detection of the fidelity number. Finally, a nonlocal fidelity marker is introduced by considering the divergence of the quantum metric. This marker is postulated as a universal indicator of quantum phase transitions, assuming the crystalline momentum remains a valid quantum number. This nonlocal marker can be interpreted as a correlation function of Wannier states, which are localized wave functions describing electronic states in a crystal. The generality and applicability of these concepts are demonstrated through the investigation of various topological insulators and topological phase transitions across different dimensions. These findings elaborate the significance of these quantities and their connection to various fundamental phenomena in condensed matter physics.

Keywords

Topological insulators; Optical absorption; Quantum geometry; Quantum phase transitions; Topological phase transitions.

Resumo

de Sousa Cruz, Antonio Lívio; Chen, Wei. **Investigando geometria quântica e criticalidade quântica por um marcador de fidelidade**. Rio de Janeiro, 2023. 49p. Dissertação de Mestrado – Departamento de Física, Pontifícia Universidade Católica do Rio de Janeiro.

A investigação da geometria quântica em semicondutores e isoladores tornou-se significativa devido às suas implicações nas características dos materiais. A noção de geometria quântica surge considerando a métrica quântica do estado de Bloch da banda de valência, que é definido a partir da sobreposição dos estados de Bloch em momentos ligeiramente diferentes. Ao integrar a métrica quântica em toda a zona de Brillouin, introduzimos uma quantidade que chamamos de número de fidelidade, que significa a distância média entre estados de Bloch adjacentes. Além disso, apresentamos um formalismo para expressar o número de fidelidade como um marcador de fidelidade local no espaço real que pode ser definido em qualquer sítio da rede. O marcador pode ser calculado diretamente diagonalizando o hamiltoniano da rede que descreve o comportamento das partículas na rede. Posteriormente, o conceito de número e marcador de fidelidade é estendido para temperatura finita utilizando a teoria de resposta linear, conectando-os a medições experimentais que envolvem analisar o poder de absorção óptica global e local quando o material é exposto à luz linearmente polarizada. Particularmente para materiais bidimensionais, a opacidade do material permite a determinação direta do número de fidelidade espectral, permitindo a detecção experimental do número de fidelidade. Finalmente, um marcador de fidelidade não local é introduzido considerando a divergência da métrica quântica. Este marcador é postulado como um indicador universal de transições de fase quântica, assumindo que o momento cristalino permanece um número quântico válido. Este marcador não local pode ser interpretado como uma função de correlação dos estados de Wannier, que são funções de onda localizadas que descrevem estados eletrônicos em um cristal. A generalidade e aplicabilidade destes conceitos são demonstradas através da investigação de vários isoladores topológicos e transições de fase topológicas em diferentes dimensões. Essas descobertas elaboram o significado dessas quantidades e sua conexão com vários fenômenos fundamentais na física da matéria condensada.

Palavras-chave

Isolantes topológicos; Absorção óptica; Geometria quântica; Transições de fase quânticas; Transições de fase topológicas.

Table of contents

1 Introduction **11**

2 Mapping quantum geometry and quantum phase transitions **15**
2.1 Introduction to Berry phases and curvatures on topological physics 15
2.2 The local fidelity marker at zero temperature 18
2.3 Formulation of a quantum phase transition detector: the non-local fidelity marker 22
2.4 Linear response theory and the finite temperature fidelity marker 24

3 Applications in one- and two-dimensional models **33**
3.1 The Su-Schrieffer-Heeger model 33
3.2 2D Chern insulator 38

4 Conclusion **45**

5 Bibliography **47**

List of figures

Figure 2.1 Schematics of the evolution of the state along a closed trajectory, which is discretized into small steps. 15

Figure 3.1 Representation of the chemical structure of *trans*-isomer of polyacetylene. 33
Figure 3.2 Schematic drawing of the two types of dimerization of the SSH model corresponding to values of $\delta t > 0$ (top) and $\delta t < 0$ (bottom). 34
Figure 3.3 Numerical results of the fidelity marker at different values of tuning parameter δt, and at zero and a finite temperature. The value in the flat region in the large part of the sample agrees with the momentum integration of the quantum metric, indicating the validity of the marker. 35
Figure 3.4 Numerical results of the nonlocal fidelity marker at several different values of δt. One sees that the nonlocal marker becomes more long ranged as the system approaches the critical point $\delta t = 0$. 36
Figure 3.5 Pictorial representation of the simulated square lattice to obtain the numerical results of this work. 39
Figure 3.6 Numerical results for the local marker in the Chern insulator at several different parameters and temperatures. For the zero temperature data, the flat region in the center gives a value that agrees with the momentum integration of quantum metric in momentum space. 41
Figure 3.7 The nonlocal fidelity marker for the Chern insulator. One sees that the marker becomes more and more long ranged at the system approaches the critical point $M = 0$. 42

Knowing your own ignorance is the first step
to enlightenment

Patrick Rothfuss, *The Wise Man's Fear.*

1
Introduction

In solids with a periodic crystalline structure, the momentum of the electrons are confined within a region in the momentum space called Brillouin zone (BZ). The BZ may be considered as a compact manifold constructed from a set of points in the momentum space, thanks to the periodicity of the lattice. The energy dispersion of the electrons manifests as multiple bands in the BZ, and from the filling of the electrons in the band structure, one classifies the materials as metals, semiconductors, or insulators. Particularly for semiconductors and insulators that have a band gap, all the bands below the chemical potential are filled and all the bands above are empty, giving rise to the notion of valence and conduction bands, respectively. Given the current interest in the exploration of insulating and semiconductor materials, especially about their topological properties, the band structure analysis becomes even more intriguing[1, 2].

Because semiconductors and insulators exhibit a band gap, their valence bands are fully occupied at zero temperature, which leads to fascinating outcomes. Firstly, the Fermi statistics ensures that the wave function $|\psi(\mathbf{k})\rangle$ of the filled valence bands at a specific momentum must be fully antisymmetric with respect to exchanging the band index. From this fully antisymmetric valence band wave function, an intriguing feature that arises is the notion of quantum geometry, defined in the following manner. The overlap of a valence band state at $\mathbf{k}$ with its neighbor at $\mathbf{k}+\delta\mathbf{k}$ is described by $|\langle\psi_{\ell\mathbf{k}}(\mathbf{k})|\psi_{\ell\mathbf{k}}(\mathbf{k}+\delta\mathbf{k})\rangle| = 1-\frac{1}{2}g_{\mu\nu}\delta k_\mu\delta k_\nu$. This overlap of Bloch states, which is often called the fidelity, defines the quantum metric $g_{\mu\nu}(\mathbf{k})$, which characterizes how these states change in the BZ manifold [3]. The concept of fidelity is based on measure how much similar is a quantum state from another one and can be related to characterization of quantum phase transition [4, 5, 6, 7, 8, 9, 10]. The quantum metric can therefore be seen as a fidelity susceptibility, in the sense that it describes how the fidelity is susceptible to the change of momentum, thereby characterizing the evolution of the fully antisymmetric valence band state over the BZ. On the other hand, from a geometrical point of view, the quantum metric brings many interesting aspects in differential geometry into the BZ manifold. For instance, one can define a geodesic running through the Hilbert space along which the valence band state changes the least. Moreover, a D-dimensional BZ can be viewed geometrically as a T^D torus, implying that it can be parameterized by a set of periodic coordinates $\mathbf{k}=\{k_1,k_2,...,k_D\}$. As

a result, the momentum integration of the quantum metric can be interpreted as the average distance between neighboring Bloch states on the manifold, leading to a number that is the main focus of this thesis that we call the fidelity number[11]. This fidelity number can be regarded as a differential geometrical property of the manifold, and moreover, we will elaborate that it is equivalent to the so-called spread of Wannier functions [12, 13, 14], an important quantity that has been investigated quite intensively within the context of first- principle calculation of band structures.

Mathematically, the quantum metric and another important concept in quantum mechanics, namely the Berry curvature, are very similar objects in the sense that one is the real part and the other the imaginary part of a more generalized concept called quantum geometric tensor. It then follows that the momentum integration of the quantum metric can be directly compared to the momentum integration of the Berry curvature, which in 2D materials is known as the Chern number [15]. Thus, comprehending the theoretical background behind the Berry curvature becomes a powerful tool to develop a similar approach for the quantum metric.

We will further demonstrate a formalism that converts the fidelity number into a function of real space positions, which is done via utilizing the identity that establishes a connection between Bloch and full wave functions [4, 5, 6, 7, 8, 9, 10]. Employing this identity, the derived expression used to obtain the fidelity number can be rewritten in a projector formalism. Consequently, this representation leads to a more concise expression that can also yield other insightful results, as the object called fidelity operator [11]. Building on a similar approach taken from the Chern number, the locality characteristic of the Wannier functions can be exploited in investigating the quantities of interest in this work.

By unifying this idea with the operator formalism, a path is paved to obtain a quantity of great interest in this work – the local fidelity marker. To introduce this marker, it becomes enriching to compare it to the Chern marker, which maps the Chern number of 2D materials in real space using the same operator formalism [16, 17, 18]. Also, in the same way as the Chern marker, the fidelity marker can be derived from the diagonal elements of the fidelity operator. The importance of this local fidelity marker lies in the fact that it facilitates the transition from momentum space to real space, offering a detailed profile of the quantum phase for each unit cell of the system. This real space representation provides a richer understanding of the system's properties and opens up new avenues for exploring and manipulating quantum phases in condensed matter systems and beyond.

Another interesting quantity we have introduced into this project comes from the consideration of the Fourier transform of the quantum metric, which results in what we call the nonlocal fidelity marker. Physically, The Fourier transform of the quantum metric is the Wannier state correlation function, which can also be displayed in real space to create a map just like the local marker. This nonlocal marker is constructed by choosing an arbitrary point of the material and profiling a map that shows the fidelity number associated to this point related to all the rest of the material. It is also very important for this work because it is potentially a universal indicator of quantum phase transitions. This suggestion is based on the fact that this nonlocal marker senses the divergence of the quantum metric when the system approaches a quantum phase transition [4, 5, 6, 7, 8, 9, 10], as long as the crystalline momentum $\mathbf{k}$ remains a valid quantum number.

The linear response theory will manifest as an important ingredient in this work, since it can be used to build an expression for the quantum metric which consider the effects of temperature [19]. The essence of this theory is to consider a semiconductor or insulator subject to a small external perturbation and determine the behavior of this system according to its response to such stimulus. To be more specific, we analyze the optical conductivity of a system subjected to an external electrical field, and relate this conductivity to the quantum metric. Our theory shows that is possible to develop a way to connect the spectral function of the fidelity number to the opacity of the material, which can be locally measured. Furthermore, it is shown that finite temperature can also be incorporated into the fidelity number, making it closer to describe realistic optical absorption experiments. In a similar way to what was done to obtain the local fidelity marker at zero temperature, our formalism can be adopted to introduce a finite temperature fidelity marker. This means that the projector formalism was also used, considering the presence of the Fermi distribution and the different way of counting energy levels. It then follows that this finite temperature fidelity marker can be directly linked to the local optical absorption power of a real material, which may be measurable by scanning thermal microscopy [20, 21, 22, 23]. As concrete applications of the quantities introduced in our work, several one-dimensional (1D) and two-dimensional (2D) lattice models will be investigated. The lattices were simulated using tight-binding Hamiltonians,numerically diagonalized in order to use their eigenstates and eigenenergies for the calculation of the markers.

The structure of the thesis is organized in the following manner. We first comment on the theoretical background of the quantum metric, and then proceed to introduce the fidelity number and fidelity marker at zero

temperature using the projector formalism. The introduction of nonlocal fidelity marker from the Fourier transform of the quantum metric is then elaborated. We then generalize all these quantities to finite temperature using a linear response theory of optical conductivity, which also links the spectral functions of fidelity number and fidelity marker to the optical absorption power of 3D materials, and the opacity of 2D materials, which clarify the experimental measurements for these quantities. For concreteness, the application of the theoretical framework to 1D and 2D lattice models of topological insulators is shown, and we will put a particular emphasis on the behavior closer to topological phase transitions. Finally, the work is concluded with a brief summary of what was done. Concluding then, commenting, in general, the results obtained after the whole process described throughout the work.

2
Mapping quantum geometry and quantum phase transitions

2.1
Introduction to Berry phases and curvatures on topological physics

Topological physics is a useful field in physics that helps to comprehend various physical phenomena and investigate the geometrical properties of materials. In recent times, its applications have become more significant, mainly due to the work of Sir Michael Berry in arranging and popularizing the theory about the Berry phase and related concepts[24].

The first concept being discussed is the *Berry phase*, also known as *geometric phase*, which is closely linked to how a state is transported adiabatically around a parameter space. To better understand this concept, a state denoted by $|\mathbf{u}_\lambda\rangle$ is used, where λ represents here the number of steps in a discrete process of the evolution of this state around a closed path, as depicted in figure 2.1.

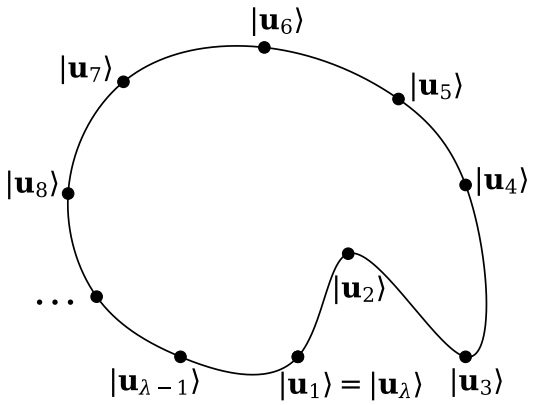

Figure 2.1: Schematics of the evolution of the state along a closed trajectory, which is discretized into small steps.

As the path is closed, the final stage of the state is essentially the same as the initial stage, so $|\mathbf{u}_\lambda\rangle = |\mathbf{u}_1\rangle$. This evolution process resulting in an accumulated global phase that is described by the Berry phase, whose formulation in discrete case is

$$\phi = -Imln\left[\langle \mathbf{u}_1|\mathbf{u}_2\rangle\langle \mathbf{u}_2|\mathbf{u}_3\rangle ...\langle \mathbf{u}_{\lambda-1}|\mathbf{u}_1\rangle\right] = -\sum_{i=1}^{\lambda-1} Imln\langle \mathbf{u}_i|\mathbf{u}_{i+1}\rangle. \qquad (2\text{-}1)$$

To express the geometric phase in a continuous way, we consider the loop to exist in a space with a parameter λ, and the state $|\mathbf{u}_\lambda\rangle$ is now a differentiable function with respect to λ. We can expand the right-hand term of eq. 2-1 by

assuming that $\mathbf{u}_\lambda$ and $\mathbf{u}_{\lambda+d\lambda}$ are related by a first-order differential equation in $d\lambda$, resulting in the form:

$$\begin{aligned} ln\langle \mathbf{u}_\lambda | \mathbf{u}_{\lambda+d\lambda} \rangle &= ln\langle \mathbf{u}_\lambda | \left(|\mathbf{u}_\lambda\rangle + d\lambda \frac{d|\mathbf{u}_\lambda\rangle}{d\lambda} + \dots \right) \\ &= ln\left(1 + d\lambda \left\langle \mathbf{u}_\lambda | \frac{d\mathbf{u}_\lambda}{d\lambda} \right\rangle + \dots \right) \\ &= d\lambda \left\langle \mathbf{u}_\lambda | \frac{d\mathbf{u}_\lambda}{d\lambda} \right\rangle + \dots, \end{aligned} \tag{2-2}$$

where we have used $\partial_\lambda = d/d\lambda$ as a shorthand notation and ignored the high-order terms in $d\lambda$ (represented by "..."). In the continuous limit, the Berry phase takes the form:

$$\phi = -Im \oint \langle \mathbf{u}_\lambda | \partial_\lambda \mathbf{u}_\lambda \rangle d\lambda, \tag{2-3}$$

where the integrand is purely imaginary, since its real part is zero. This can be further simplified to:

$$\phi = \oint \langle \mathbf{u}_\lambda | i\partial_\lambda \mathbf{u}_\lambda \rangle d\lambda, \tag{2-4}$$

which was originally formulated by Berry in 1984[25]. An important characteristic of it is its *gauge invariance* modulo 2π, i. e., under a gauge transformation it takes the form $\tilde{\phi} = \phi + 2\pi n$, where n is an integer number, and this is why it's called a phase.

It is worth noting that in the expression for the geometrical phase given in equation 2-4, the integrand on the right-hand side is a mathematical concept known as the *Berry connection* or *Berry potential* [24]. The Berry connection, denoted by $\mathbf{A}(\lambda)$, is a vector-valued function defined as:

$$\mathbf{A}(\lambda) = \langle \mathbf{u}_\lambda | i\partial_\lambda \mathbf{u}_\lambda \rangle. \tag{2-5}$$

It should be emphasized that unlike the Berry phase (when it's considered as a phase angle), the Berry connection is *not* a gauge-invariant quantity, then it depends on the choice of a phase[25]. And, it is also very important for the construction of the concept in the following section.

Berry curvature

The *Berry curvature* is a significant quantity in the understanding of various phenomena in quantum mechanics, such as the quantum Hall effect, topological insulators, and topological phases of matter[1, 26]. It arises from the study of the geometric properties of the wave function.

To extend the previous notation to a two-dimensional parameter space, the vectors $|\mathbf{u}_{\boldsymbol{\lambda}}\rangle$ are now functions of $\boldsymbol{\lambda} = \{\lambda_x, \lambda_y\}$. Similarly, there is a formulation for a two-dimensional Berry connection vector $\mathbf{A} = \{A_x, A_y\}$, which also depends on $\boldsymbol{\lambda}$, given by:

$$A_\mu = \langle \mathbf{u}_{\boldsymbol{\lambda}} | i\partial_\mu \mathbf{u}_{\boldsymbol{\lambda}} \rangle, \tag{2-6}$$

where $\partial_\mu = \partial/\partial\lambda_\mu$ and the symbol μ is used here just as a generalization to represent a direction, which in this case can be $\{x, y\}$.

This way, the Berry curvature can be defined as the curl of the Berry connection[25]. Then, considering a surface S surrounded by its contour C, it can be defined as

$$\boldsymbol{\Omega}_{xy} = \partial_x A_y - \partial_y A_x, \tag{2-7}$$

and is possible to proceed with its representation, writing it in a generalized form, doing

$$\begin{aligned} \boldsymbol{\Omega}_{\mu\nu} = \partial_\mu A_\nu - \partial_\nu A_\mu &= \partial_\mu \langle \mathbf{u} | i\partial_\nu \mathbf{u} \rangle - \partial_\nu \langle \mathbf{u} | i\partial_\mu \mathbf{u} \rangle \\ &= \langle \partial_\mu \mathbf{u} | i\partial_\nu \mathbf{u} \rangle + \cancel{\langle \mathbf{u} | i\partial_\mu \partial_\nu \mathbf{u} \rangle} \\ &- \langle \partial_\nu \mathbf{u} | i\partial_\mu \mathbf{u} \rangle - \cancel{\langle \mathbf{u} | i\partial_\nu \partial_\mu \mathbf{u} \rangle} \\ &= -Im\langle \partial_\mu \mathbf{u} | \partial_\nu \mathbf{u} \rangle + Im\langle \partial_\nu \mathbf{u} | \partial_\mu \mathbf{u} \rangle, \end{aligned} \tag{2-8}$$

where, knowing that $\langle \partial_\nu \mathbf{u} | \partial_\mu \mathbf{u} \rangle^* = \langle \partial_\mu \mathbf{u} | \partial_\nu \mathbf{u} \rangle$, it is certain that $Im\langle \partial_\nu \mathbf{u} | \partial_\mu \mathbf{u} \rangle = -Im\langle \partial_\mu \mathbf{u} | \partial_\nu \mathbf{u} \rangle$, then it is finally possible to reach

$$\boldsymbol{\Omega}_{\mu\nu} = \partial_\mu A_\nu - \partial_\nu A_\mu = -2Im\langle \partial_\mu \mathbf{u} | \partial_\nu \mathbf{u} \rangle. \tag{2-9}$$

Once the Berry curvature was introduced, now it is possible to comment about the "Berry flux" Φ_S, through a surface S surrounded by a contour P

$$\begin{aligned} \Phi_S &= \int_S \Omega(\lambda) dS = \oint_P \mathbf{A} \cdot d\lambda \\ &= \phi_P \end{aligned} \tag{2-10}$$

which is shown to be equal to the Berry phase around P through the use of the Stokes' theorem. The calculations presented in Eq. 2-10 hold significant importance in the formulation of the upcoming theorem, as discussed in the following section.

The Chern number

The Chern theorem, which is also referred to as the Chern-Gauss-Bonnet theorem, is a crucial outcome in differential geometry that links the geometry of a smooth manifold to its topology. Its main idea is that the total curvature

of a manifold is connected to a specific differential form called the Chern form, which is determined by the curvature of the manifold's tangent bundle. This connection is expressed as an integral over the manifold. This procedure is mathematically described by the following expressions:

$$\oint_S \mathbf{\Omega} \cdot dS = 2\pi C, \tag{2-11}$$

and then, employing the Stoke's theorem,

$$\int_S \mathbf{\Omega} \cdot dS := \oint_P \mathbf{A} \cdot d\lambda. \tag{2-12}$$

The significance of the Chern number C lies in its association with the quantized Hall conductance[15] and its prominent role as an example of topological order. The main objective of this work is to introduce the concept of quantum metric and the fidelity number, which exhibit a remarkable resemblance to the Berry curvature and the Chern number discussed in the previous section, as detailed below.

2.2 The local fidelity marker at zero temperature

The study of quantum geometric properties is a crucial aspect of understanding the behavior of materials at the nanoscale. The primary aim of this work is to explore the integration of the quantum metric in momentum space for individual lattice sites. This approach enables a comprehensive analysis of the material's quantum geometric properties on a site-by-site basis, providing a detailed profile of the behavior of these properties throughout the entire material.

Traditionally, the characterization of materials' geometric properties has been limited to global measures such as the curvature and torsion of a surface or the Euler characteristic of a manifold. However, in recent years, there has been a growing interest in studying the geometric properties of materials at the atomic scale, where quantum mechanics plays a dominant role. This has led to the development of the concept of quantum geometry, which describes the behavior of quantum systems in terms of their geometric properties.

In this context, the integration of the quantum metric in momentum space for each site on a lattice provides a powerful tool for analyzing the behavior of materials at the nanoscale. This approach allows for a more detailed and accurate description of the quantum geometric properties of the material, taking into account the local variations in these properties that can arise from the complex interactions between atoms.

Overall, this work demonstrates the potential of the integration of the

quantum metric in momentum space for understanding the behavior of materials at the nanoscale. The ability to analyze the material's quantum geometric properties on a site-by-site basis provides a more comprehensive understanding of the material's behavior, which could have significant implications for the development of new materials with tailored quantum properties for use in a wide range of applications.

Gapped insulating materials as TIs can be characterized by a Hamiltonian, denoted by $\mathbf{H}$, in momentum space, which satisfies the secular equation $\mathbf{H}|\psi_{\ell\mathbf{k}}\rangle = \epsilon_{\ell\mathbf{k}}|\psi_{\ell\mathbf{k}}\rangle$. Here, $|\psi_{\ell\mathbf{k}}\rangle$ represents the Bloch eigenstates, $\epsilon_{\ell\mathbf{k}}$ are their respective eigenenergies and is important to mention that the letters ℓ, n and m will be used hereafter to indicate all the bands of the material, the valence bands and the conduction bands respectively. Geometrically, the *quantum metric* in the Hilbert space can be defined by the overlap of the eigenstate at momentum $\mathbf{k}$ with itself at a different momentum $\mathbf{k}+\delta\mathbf{k}$

$$|\langle\psi_{\ell\mathbf{k}}(\mathbf{k})|\psi_{\ell\mathbf{k}}(\mathbf{k}+\delta\mathbf{k})\rangle| = 1 - \frac{1}{2}g_{\mu\nu}\delta k_\mu \delta k_\nu, \tag{2-13}$$

which gives rise to the expression[3]

$$g_{\mu\nu}(\mathbf{k}) = \frac{1}{2}\langle\partial_\mu\psi_{\ell\mathbf{k}}|\partial_\nu\psi_{\ell\mathbf{k}}\rangle + \frac{1}{2}\langle\partial_\nu\psi_{\ell\mathbf{k}}|\partial_\mu\psi_{\ell\mathbf{k}}\rangle - \langle\partial_\mu\psi_{\ell\mathbf{k}}|\psi_{\ell\mathbf{k}}\rangle\langle\psi_{\ell\mathbf{k}}|\partial_\nu\psi_{\ell\mathbf{k}}\rangle. \tag{2-14}$$

This expression is gauge invariant, just like the Berry curvature.. Taking the periodic part of the Bloch state for all the bands $u_{\ell\mathbf{k}}(\mathbf{r}) = e^{-i\mathbf{k}\cdot\mathbf{r}}\psi_{\ell\mathbf{k}}(\mathbf{r}) = \langle\mathbf{r}|u_{\ell\mathbf{k}}\rangle$, it satisfies the condition $u_{\ell\mathbf{k}}(\mathbf{r}) = u_{\ell\mathbf{k}}(\mathbf{r}+\mathbf{R})$, that means it is invariant under a translation to a different position represented by the Bravais vector $\mathbf{R}$. Then, to find the correspondent Wannier state $|\mathbf{R}_\ell\rangle$ of each Bloch state $|u_{\ell\mathbf{k}}\rangle$, and contrariwise, is necessary to do a transformation using the relations

$$|u_{\ell\mathbf{k}}\rangle = \sum_{\mathbf{R}} e^{-i\mathbf{k}\cdot(\mathbf{r}-\mathbf{R})}|\mathbf{R}_\ell\rangle,\ |\mathbf{R}_\ell\rangle = \sum_{\mathbf{R}} e^{-i\mathbf{k}\cdot(\mathbf{r}-\mathbf{R})}|u_{\ell\mathbf{k}}\rangle, \tag{2-15}$$

where the obtained Wannier state corresponds to a Wannier function $W_\ell(\mathbf{r}-\mathbf{R}) = \langle\mathbf{r}|\mathbf{R}_\ell\rangle$, which has the feature of been high localized function on the position $\mathbf{R}$.

To describe the quantum geometry of insulators and semiconductors, one must respect the Fermi statistics of electrons in a multiband system. This means that the right quantity to begin with is the fully antisymmetric Bloch state constructed out of all valence bands

$$|\psi^-(\mathbf{k})\rangle = \frac{1}{\sqrt{N^-!}}\epsilon^{12\ldots N^-}|u_{1\mathbf{k}}\rangle|u_{2\mathbf{k}}\rangle\ \ldots\ |u_{N^-\mathbf{k}}\rangle, \tag{2-16}$$

where the eigenvectors $|u_{n\mathbf{k}}\rangle$ of the N^- valence bands forms its basis. A straightforward calculation leads to an expression for the quantum metric of this fully antisymmetric state [27]

$$\begin{aligned} g_{\mu\nu}(\mathbf{k}) =& \frac{1}{2}\langle\partial_\mu\psi^-|\partial_\nu\psi^-\rangle + \frac{1}{2}\langle\partial_\nu\psi^-|\partial_\mu\psi^-\rangle - \langle\partial_\mu\psi^-|\psi^-\rangle\langle\psi^-|\partial_\nu\psi^-\rangle \\ =& \frac{1}{2}\sum_{nm}\left[\langle\partial_\mu u_n|u_m\rangle\langle u_m|\partial_\nu u_n\rangle + \langle\partial_\nu u_n|u_m\rangle\langle u_m|\partial_\mu u_n\rangle\right]. \end{aligned} \tag{2-17}$$

Thus, a similar process used to find the Chern number is now used to find the *fidelity number*, what means that it can be obtained by integrating the quantum metric in eq.(2-17) over momentum as

$$\begin{aligned} \mathrm{G}_{\mu\nu} &= \int \frac{d^D\mathbf{k}}{(2\pi)^D} g_{\mu\nu}(\mathbf{k}) \\ &= \frac{1}{2\hbar^2}\int \frac{d^D\mathbf{k}}{(2\pi)^D}\sum_{nm}\left[\langle\psi_{n\mathbf{k}}|\hat{\mu}|\psi_{m\mathbf{k}}\rangle\,\langle\psi_{m\mathbf{k}}|\hat{\nu}|\psi_{n\mathbf{k}}\rangle + (\mu\leftrightarrow\nu)\right] \end{aligned} \tag{2-18}$$

and is possible to see that the expression for the quantum metric is different to the previously shown, and this happens by the using of the the first part of the identity [13, 14, 18, 28, 29, 30]

$$\begin{aligned} i\,\langle u_m|\partial_\mu u_n\rangle &= \frac{1}{\hbar}\,\langle\psi_{m\mathbf{k}}|\hat{\mu}|\psi_{n\mathbf{k}}\rangle \\ &= \sum_{\mathbf{R}}\frac{e^{i\mathbf{k}\cdot\mathbf{R}}}{\hbar}\langle 0_m|\hat{\mu}|\mathbf{R}_n\rangle = \sum_{\mathbf{R}}\frac{e^{-i\mathbf{k}\cdot\mathbf{R}}}{\hbar}\langle\mathbf{R}_m|\hat{\mu}|0_n\rangle \end{aligned}$$

which one is basically a representation to the link between the Bloch and Wannier states by Fourier transformation with $m \neq n$, and thanks to it, the constant $\hbar$ appear in the equations. And the operators $\hat{\mu}$ and $\hat{\nu}$ denotes here the position operators for the whole lattice in each direction, which are defined by

$$\begin{aligned} \hat{\mu} &= \sum_{\mathbf{r},\sigma}|\mathbf{r},\sigma\rangle\mu_{\mathbf{r}}\langle\mathbf{r},\sigma| \equiv \sum_{\mathbf{r}}|\mathbf{r}\rangle\mu_{\mathbf{r}}\langle\mathbf{r}|, \\ \hat{\nu} &= \sum_{\mathbf{r},\sigma}|\mathbf{r},\sigma\rangle\nu_{\mathbf{r}}\langle\mathbf{r},\sigma| \equiv \sum_{\mathbf{r}}|\mathbf{r}\rangle\nu_{\mathbf{r}}\langle\mathbf{r}|, \end{aligned} \tag{2-19}$$

where σ represents here any internal degree of freedom that can be present in the unit cell, and $\mathbf{r}$ is the position of each site. Then, the next step is separate the momentum integration in two integrals, one in $\mathbf{k}$ and other in $\mathbf{k}'$, dividing them by $(\hbar/a)^D$, where a is the distance between the sties, leading to

$$\begin{aligned} \mathrm{G}_{\mu\nu} = \frac{\hbar^{D-2}}{2a^D}\int \frac{d^D\mathbf{k}}{(2\pi\hbar/a)^D}\int \frac{d^D\mathbf{k}'}{(2\pi\hbar/a)^D}\times \\ \times\sum_{nm}\left[\langle\psi_{n\mathbf{k}}|\hat{\mu}|\psi_{m\mathbf{k}'}\rangle\,\langle\psi_{m\mathbf{k}'}|\hat{\nu}|\psi_{n\mathbf{k}}\rangle + (\mu\leftrightarrow\nu)\right], \end{aligned} \tag{2-20}$$

in which, the integrals in "different" variables are used to separate the integration over the valence and conduction bands, where $\mathbf{k}$ is related to the valence band and $\mathbf{k}'$ to the conduction band. Moreover, the second line can be at-

tributed to the fact that the matrix elements become zero when k is not equal to k'. The constant $(\hbar/a)^D$, where a^D is basically a D-dimensional volume of the primitive cell, was putted here by an algebraism aiming to relate the Bloch states to the Wannier states, as shown in the second part of the identity in eq.(2-19). This way, the expression for the fidelity number can be manipulated to be expressed in terms of the Wannier states and takes the form

$$\mathrm{G}_{\mu\nu} = \sum_{nm}\sum_{\mathbf{R}} \frac{1}{2}[\langle \mathbf{0}_n|\hat{\mu}|\mathbf{R}_m\rangle\langle \mathbf{R}_m|\hat{\nu}|\mathbf{0}_n\rangle + (\mu \leftrightarrow \nu)]. \tag{2-21}$$

Then, the fidelity number can also be written in terms of the Wannier functions as

$$\mathrm{G}_{\mu\nu} = \sum_{nm}\sum_{\mathbf{R}} \frac{1}{2}\int d\mathbf{r}\int d\mathbf{r}'[\mu_{\mathbf{r}} W_n^*(\mathbf{r})W_m(\mathbf{r}-\mathbf{R})\times \\ \times \nu_{\mathbf{r}'} W_m^*(\mathbf{r}'-\mathbf{R})W_m(\mathbf{r}') + (\mu \leftrightarrow \nu)], \tag{2-22}$$

which ones will be integrated over the positions $\mathbf{r}$ and $\mathbf{r}'$ of different atoms, to count the contribution over each site of the system.

Supposing now that H is a tight-binding Hamiltonian for a D-dimensional lattice expressed as $\mathrm{H} = \sum_{\mathbf{r}\mathbf{r}'\sigma\sigma'} t_{\mathbf{r}\mathbf{r}'\sigma\sigma'} c^\dagger_{\mathbf{r}\sigma} c_{\mathbf{r}'\sigma'}$, where $\mathbf{r}$ is the positions of the sites, σ represents any degree of freedon, such as spin, and $t_{\mathbf{r}\mathbf{r}'\sigma\sigma'}$ is the hopping term. Diagonalizing this Hamiltonian by the secular equation leads to its eigenenergies and eigenstates according to $\mathrm{H}\,|\epsilon_\ell\rangle = \epsilon_\ell|\epsilon_\ell\rangle$. It is then employed a projector formalism to rewrite Eq. 2-20 completely in terms of these lattice eigenstates. This is done by identifying the momentum integration of the projectors of momentum eigenstates with the sum of lattice eigenstates [18]

$$\begin{aligned} \hat{\mathrm{P}} &= \sum_n \int_{BZ} \frac{d^D\mathbf{k}}{(2\pi\hbar/a)^D} |\psi_{n\mathbf{k}}\rangle\langle\psi_{n\mathbf{k}}| \rightarrow \sum_n |\epsilon_n\rangle\langle\epsilon_n|, \\ \hat{\mathrm{Q}} &= \sum_m \int_{BZ} \frac{d^D\mathbf{k}'}{(2\pi\hbar/a)^D} |\psi_{m\mathbf{k}'}\rangle\langle\psi_{m\mathbf{k}'}| \rightarrow \sum_m |\epsilon_m\rangle\langle\epsilon_m|. \end{aligned} \tag{2-23}$$

The projector $\hat{\mathrm{P}}$ is calculated using the valence band eigenstates, while $\hat{\mathrm{Q}}$ is calculated using the conduction band eigenstates and both of them can be related by $\hat{\mathrm{P}} = \mathrm{I} - \hat{\mathrm{Q}}$. Here is possible to see that the earlier introduction of the term $(\hbar/a)^D$ fits with the intention to use these operators in the calculations of this work, turning them more practical.

When introducing this projectors tho build a new formulation for calculations, the expressions takes a more compact form. This way, knowing that the projectors are matrices, the main diagonal elements obtained after make the operations due the process to find the fidelity number will be the value

of this quantity for each site of the lattice. Then, the sum is replaced by the trace of the resultant matrix and the calculation of the fidelity number can be denoted as

$$\mathrm{G}_{\mu\nu} = \frac{\hbar^{D-2}}{a^D N}\,\mathrm{Tr}\left[\frac{1}{2}\left(\hat{\mathrm{P}}\hat{\mu}\hat{\mathrm{Q}}\hat{\nu} + \hat{\mathrm{P}}\hat{\nu}\hat{\mathrm{Q}}\hat{\mu}\right)\right], \tag{2-24}$$

where $\hat{\mu}$ and $\hat{\nu}$ are the position operators related to two arbitrary directions and N is the number of unit cells. Now, the expression of eq.(2-24) can be rewritten calling the trace as the sum over the position of each site

$$\mathrm{G}_{\mu\nu} = \frac{\hbar^{D-2}}{a^D N}\,\mathrm{Tr}\left[\frac{1}{2}\left(\hat{\mathrm{P}}\hat{\mu}\hat{\mathrm{Q}}\hat{\nu}\hat{\mathrm{P}} + \hat{\mathrm{P}}\hat{\nu}\hat{\mathrm{Q}}\hat{\mu}\hat{\mathrm{P}}\right)\right] = \frac{1}{N}\sum_{\mathbf{r}}\mathrm{G}_{\mu\nu}(\mathbf{r}), \tag{2-25}$$

considering that only the main diagonal elements are necessary now, these elements leads to another quantity named local fidelity marker, whose representation is

$$\begin{aligned}\mathrm{G}_{\mu\nu}(\mathbf{r}) &= \frac{\hbar^{D-2}}{a^D}\sum_{\sigma}\left\langle \mathbf{r},\sigma\left|\left[\frac{1}{2}\left(\hat{P}\hat{\mu}\hat{Q}\hat{\nu}\hat{P} + \hat{P}\hat{\nu}\hat{Q}\hat{\mu}\hat{P}\right)\right]\right|\mathbf{r},\sigma\right\rangle \\ &\equiv \frac{\hbar^{D-2}}{a^D}\left\langle \mathbf{r}\left|\left[\frac{1}{2}\left(\hat{P}\hat{\mu}\hat{Q}\hat{\nu}\hat{P} + \hat{P}\hat{\nu}\hat{Q}\hat{\mu}\hat{P}\right)\right]\right|\mathbf{r}\right\rangle,\end{aligned} \tag{2-26}$$

whose part of it, denoted as $\frac{1}{2}\left(\hat{\mathrm{P}}\hat{\mu}\hat{\mathrm{Q}}\hat{\nu}\hat{\mathrm{P}} + \hat{\mathrm{P}}\hat{\nu}\hat{\mathrm{Q}}\hat{\mu}\hat{\mathrm{P}}\right)$, will be treated here separately and called as *fidelity operator*

$$\hat{\mathrm{G}}_{\mu\nu} \equiv 1/2[\hat{\mathrm{P}}\hat{\mu}\hat{\mathrm{Q}}\hat{\nu}\hat{\mathrm{P}} + \hat{\mathrm{P}}\hat{\nu}\hat{\mathrm{Q}}\hat{\mu}\hat{\mathrm{P}}]. \tag{2-27}$$

It is interesting to mention that, from eq.(2-25) onwadrs, the operator $\hat{\mathrm{G}}_{\mu\nu}$ is written multiplied by $\hat{\mathrm{P}}$ by the right. This modification is made based on observation of numerical results, and is essential to observe the profile of the marker offered by its main diagonal.

The main goal of the present work is to show that the integration of quantum metric in momentum space can be defined for each site on a lattice using the fidelity operator in Eq. 2-27, which allows to show the geometrical properties of the material site by site on the lattice. It will be seen in the next section how this is done explicitly.

2.3 Formulation of a quantum phase transition detector: the non-local fidelity marker

Focusing on the zero temperature regime, the fact that the quantum metric diverges near a phase transition can be exploited in another way, namely by integrating the metric over momentum space to yield the fidelity number, and then express it in real space to give a fidelity marker. In addition, the divergent quantum metric also gives rise to the formulation of a non-local fidelity marker which is proposed to be able to be used as a universal indicator

for quantum phase transitions. These quantities will be introduced in this section.

This marker works relating a lattice site in position $\mathbf{r}$ to another observed site in position $\mathbf{r}+\mathbf{R}'$, offering a correlation between them. Therefore, since the local marker is obtained by the diagonal elements of the fidelity operator matrix

$$\mathrm{G}_{\mu\nu}(\mathbf{r}) = \langle \mathbf{r}|\, \hat{\mathrm{G}}_{\mu\nu}\, |\mathbf{r}\rangle, \tag{2-28}$$

This quantity referred to as the fidelity marker. Physically, in a translationally invariant system, ideally it should give a constant on every lattice site, and the constant is equal to the fidelity number. In this manner, the fidelity number has been inscribed into a real space object. The second quantity under consideration is the Fourier transform of the quantum metric

$$\tilde{g}_{\mu\nu}(\mathbf{R}') = \int \frac{d^D\mathbf{k}}{(2\pi)^D} g_{\mu\nu}(\mathbf{k}) e^{i\mathbf{k}\cdot\mathbf{R}'}. \tag{2-29}$$

The motivation of considering this Fourier transform is that because the quantum metric generally diverges somewhere in the momentum space near a phase transition, it will likely diverge with a peak shape, and hence the Fourier transform of the peak should give a quantity in real space that carries some information about the diverging quantum metric. Thus, the suggestion proposed by this work is that this Fourier transform may serve as a universal indicator for any quantum phase transitions. In fact, one can use the Wannier state formalism to write this Fourier transform into a form that looks like a correlator between Wannier states. This is done by first using the same formalism as Eq. 2-18, yielding

$$\begin{aligned}\tilde{g}_{\mu\nu}(\mathbf{R}') = \frac{\hbar^{D-2}}{a^D} \sum_n \sum_m \int \frac{d^D\mathbf{k}}{(2\pi\hbar/a)^D} \int \frac{d^D\mathbf{k}'}{(2\pi\hbar/a)^D} \times \\ \times \frac{1}{2}\left[\langle\psi_{n\mathbf{k}}|\hat{\mu}|\psi_{m\mathbf{k}'}\rangle \langle\psi_{m\mathbf{k}'}|\hat{\nu}|\psi_{n\mathbf{k}}\rangle\, e^{i\mathbf{k}\cdot\mathbf{R}'} + (\mu \leftrightarrow \nu)\right],\end{aligned} \tag{2-30}$$

where using the Bloch function property of periodicity, due to the crystalline aspect of the lattice, implies that $\langle\mathbf{r}|\psi_{n\mathbf{k}}\rangle e^{i\mathbf{k}\cdot\mathbf{R}'} \equiv \langle\mathbf{r}+\mathbf{R}'|\psi_{n\mathbf{k}}\rangle$ is a valid relation for the projection of the wave function. Hence, through using again the identity in eq. 2-19, it can be rewritten as

$$\tilde{g}_{\mu\nu}(\mathbf{R}') = \sum_{nm} \sum_{\mathbf{R_1}} \frac{1}{2}\left[\langle\mathbf{0}_n|\hat{\mu}|\mathbf{R_1}_m\rangle \langle(\mathbf{R_1}+\mathbf{R}')_m|\hat{\nu}|\mathbf{0}_n\rangle + (\mu \leftrightarrow \nu)\right], \tag{2-31}$$

where $\mathbf{R_1}$ is the parameter related to the use of such identity, and now, is

possible to present this correlation function in terms of the Wannier functions

$$\tilde{g}_{\mu\nu}(\mathbf{R}') = \sum_{nm}\sum_{\mathbf{R_1}} \frac{1}{2}\int d\mathbf{r}\int d\mathbf{r}'[\mu_{\mathbf{r}} W_n^*(\mathbf{r}) W_m\left(\mathbf{r}-\mathbf{R_1}\right)\nu_{\mathbf{r}'}\times \\ \times W_m^*\left(\mathbf{r}'-\mathbf{R_1}-\mathbf{R}'\right) W_n\left(\mathbf{r}'\right)+(\mu\leftrightarrow\nu)]. \quad (2\text{-}32)$$

It will behaves as a superposition of the Wannier functions where, out of the thermodynamic limit, it will only be different from zero in the positions of the lattice sites. Then, gives rise to the *non-local fidelity marker* $\mathrm{G}_{\mu\nu}(\mathbf{r}+\mathbf{R}') = \langle(\mathbf{r}+\mathbf{R}')|\,\hat{\mathrm{G}}_{\mu\nu}\,|\mathbf{r}\rangle$, which $\lim_{N\to+\infty} \mathrm{G}_{\mu\nu}(\mathbf{r}+\mathbf{R}') = \tilde{g}_{\mu\nu}(\mathbf{R}')$, and will correspond to the $(\mathbf{r}+\mathbf{R}',\mathbf{r})$-th off-diagonal matrix elements of the fidelity operator matrix.

Turning back to the formalism used in the present work, the non-local fidelity marker is denoted by

$$\mathrm{G}_{\mu\nu}(\mathbf{r}+\mathbf{R}',\mathbf{r}) = \frac{\hbar^{D-2}}{a^D}\,\mathrm{Re}\left\{\sum_{\sigma}\left\langle \mathbf{r}+\mathbf{R}',\sigma\left|\left[\frac{1}{2}\hat{P}\hat{\mu}\hat{Q}\hat{\nu}\hat{P}+(\mu\leftrightarrow\nu)\right]\right|\mathbf{r},\sigma\right\rangle\right\} \\ \equiv \frac{\hbar^{D-2}}{a^D}\,\mathrm{Re}\left\{\left\langle \mathbf{r}+\mathbf{R}'\left|\left[\frac{1}{2}\hat{P}\hat{\mu}\hat{Q}\hat{P}+(\mu\leftrightarrow\nu)\right]\right|\mathbf{r}\right\rangle\right\}, \quad (2\text{-}33)$$

using the real part of the terms in the trace and ignoring again the degree of freedom represented by σ, the similarity with the expression for the local fidelity marker is clear.

2.4 Linear response theory and the finite temperature fidelity marker

Linear response theory is a branch of physics that deals with the relationship between a system's response to an external stimulus and the strength of that stimulus. The theory provides a mathematical framework for describing the behavior of a wide range of physical systems, including mechanical, electrical, and biological systems. In linear response theory, the response of a system to a small perturbation is assumed to be linearly proportional to the strength of the perturbation. This means that if the system is subject to a small external force or disturbance, its response will be directly proportional to the strength of the force or disturbance. This assumption is valid when the perturbation is small enough that it does not significantly alter the behavior of the system. Linear response theory is used to study a wide range of physical phenomena, including the behavior of materials under stress, the dynamics of chemical reactions, the response of biological systems to environmental changes, and the properties of complex systems such as fluids

and plasmas. It is also used in the development of control systems, where the goal is to manipulate a system's response to achieve a desired outcome.

In this work, the aim is to elaborate an expression for the fidelity marker considering temperature and connecting it to measurable quantities, is proposed through the linear response theory. The first step to its development is denote the quantum metric spectral function of a system subjected to an oscillating electrical field [19]

Relations with experimentally measurable quantities

The connection with experimental results comes from the optical response of the material. This is made considering the system affected by an oscillating electric field E_μ, which induces a current that can be described by a current operator in momentum space $\hat{j}_\mu = e\,\partial_\mu \mathrm{H}$ [31], where H is the Hamiltonian in momentum space $\mathbf{k}$ for a system with a D-dimensional volume of its unit cell equal to a^D and e is the electron charge. Once the induced current can be obtained, using the linear response theory for a non-interacting system [32] it is possible to obtain the finite temperature *longitudinal optical conductivity*. To formulate the conductivity in momentum $\mathbf{k}$, is necessary to start with the current operator in the second quantization form

$$\hat{j}_\mu(\mathbf{k}) = e \sum_{\ell<\ell'} \langle u_\ell|\partial_\mu \mathrm{H}|u_{\ell'}\rangle c^\dagger_{\ell\mathbf{k}} c_{\ell'\mathbf{k}}. \tag{2-34}$$

The formalism can be applied to interacting systems as well, $\mathrm{H} + \mathrm{H}'$, where H' is the interacting Hamiltonian. Then, in the most general case, , the time-evolution of the current operator is givem by

$$\hat{j}_\mu(\mathbf{k}, t) = e^{i(\mathrm{H}+\mathrm{H}')t} \hat{j}_\mu(\mathbf{k}) e^{-i(\mathrm{H}+\mathrm{H}')t}. \tag{2-35}$$

With the purpose of calculate the current at momentum $\mathbf{k}$ caused by applying an electromagnetic wave, the perturbation is described by the minimal coupling. Assuming the electric field $\vec{E}$ along μ direction, the Hamiltonian is given by

$$\mathrm{H}' = -e\vec{A}\cdot\vec{v} = -eA_\mu \partial_\mu \mathrm{H}, \tag{2-36}$$

which is write in term of the vector potential. In what follows, the speed of the light c, $\hbar$ and lattice constant a will be ignored ($\hbar = c = a = 1$), but they will be restore later. Then, denoting the oscillating electric field of the electromagnetic wave as

$$\begin{aligned} \vec{E} &= \hat{\mu} E_\mu(t) = \hat{\mu} E_0 e^{-i\omega t} \\ E_\mu(t) &= -\frac{\partial A_\mu}{\partial t} = i\omega A_\mu \end{aligned} \tag{2-37}$$

where the time-dependent external electric field $E_\mu(t)$ can be directly related to the component of the vector potential

$$A_\mu = -\frac{i}{\omega} E_\mu(t). \tag{2-38}$$

So, in second quantization, the perturbation caused by the electromagnetic wave is

$$\begin{aligned} \delta \mathrm{H}(\mathbf{k}) &= -eA_\mu \sum_{\ell<\ell'} \langle u_\ell | \partial_\mu \mathrm{H} | u_{\ell'} \rangle c^\dagger_{\ell\mathbf{k}} c_{\ell'\mathbf{k}} \\ &= \frac{i}{\omega} eE_\mu \sum_{\ell<\ell'} \langle u_\ell | \partial_\mu \mathrm{H} | u_{\ell'} \rangle c^\dagger_{\ell\mathbf{k}} c_{\ell'\mathbf{k}} = \frac{i}{\omega} E_\mu \hat{j}_\mu(\mathbf{k}). \end{aligned} \tag{2-39}$$

Likewisely, the time evolution of it is:

$$\delta \mathrm{H}(\mathbf{k}, t) = \frac{i}{\omega} E_\mu(t) \hat{j}_\mu(\mathbf{k}, t), \tag{2-40}$$

which is used to obtain the conductivity

$$\langle \hat{j}_\mu(\mathbf{k}, t) \rangle = \sigma_{\mu\mu}(\mathbf{k}, t) E_\mu(t), \tag{2-41}$$

where $\langle \dots \rangle$ is the ensemble average. Within linear response theory, it is calculated by:

$$\begin{aligned} \langle \hat{j}_\mu(\mathbf{k}, t) \rangle &= -i \int_{-\infty}^{t} dt' \langle [\hat{j}_\mu(\mathbf{k}, t), \delta \mathrm{H}(\mathbf{k}, t')] \rangle \\ &= -i \int_{-\infty}^{t} dt' \langle [\hat{j}_\mu(\mathbf{k}, t), \hat{j}_\mu(\mathbf{k}, t')] \rangle \left(\frac{i}{\omega}\right) E_\mu(t') \\ &= -i \int_{-\infty}^{t} dt' \langle [\hat{j}_\mu(\mathbf{k}, t), \hat{j}_\mu(\mathbf{k}, t')] \rangle \left(\frac{i}{\omega}\right) E_\mu(t) e^{i\omega(t-t')} \end{aligned} \tag{2-42}$$

What leads to define a frequency-dependent conductivity

$$\tilde{\sigma}_{\mu\mu}(\mathbf{k}, \omega) = \left(\frac{i}{\omega}\right)(-i) \int_{-\infty}^{t} dt' e^{i\omega(t-t')} \langle [\hat{j}_\mu(\mathbf{k}, t), \hat{j}_\mu(\mathbf{k}, t')] \rangle. \tag{2-43}$$

The linear response theory can be generalized to finite temperature using the Matsubara formalism; which amounts to calculating

$$\Pi_{\mu\mu}(\mathbf{k}, i\omega) = \int_0^\beta d\tau e^{i\omega\tau} \Pi_{\mu\mu}(\mathbf{k}, \tau), \tag{2-44}$$

where,

$$\Pi_{\mu\mu}(\mathbf{k}, \tau) = -\langle \mathrm{T}_\tau \hat{j}(\mathbf{k}, \tau) \hat{j}(\mathbf{k}, 0) \rangle. \tag{2-45}$$

Assuming no interaction is present, i.e. $\mathrm{H}' = 0$, and after analytical continuation $i\omega \to \omega$, the usual Green's function and frequency sum calculation gives

$$\Pi_{\mu\mu}(\mathbf{k}, \omega) = \sum_{\ell<\ell'} \langle u_\ell | \partial_\mu \mathrm{H} | u_{\ell'} \rangle \langle u_{\ell'} | \partial_\mu \mathrm{H} | u_\ell \rangle \frac{f(E_\ell) - f(E_{\ell'})}{\omega + E_\ell - E_{\ell'} + + i\eta}, \tag{2-46}$$

where η is a small artificial broadening. And back to the formalism above, the complex conductivity is written as

$$\tilde{\sigma}_{\mu\mu}(\mathbf{k}, \omega) = \frac{i}{\omega} \Pi_{\mu\mu}(\mathbf{k}, \omega), \tag{2-47}$$

and then, it is necessary to take its real part

$$\begin{aligned}\sigma_{\mu\mu}(\mathbf{k},\omega) &= \text{Re }\tilde{\sigma}_{\mu\mu}(\mathbf{k},\omega) = \text{Re}\left(\frac{i}{\omega}\Pi_{\mu\mu}(\mathbf{k},\omega)\right) = -\frac{\text{Im }\Pi_{\mu\mu}(\mathbf{k},\omega)}{\omega} \\ &= -\frac{1}{\omega}\sum_{\ell<\ell'}\langle u_\ell|\partial_\mu \mathrm{H}|u_{\ell'}\rangle\langle u_{\ell'}|\partial_\mu \mathrm{H}|u_\ell\rangle[f(E_\ell)-f(E_{\ell'})]\frac{-\eta}{(\omega+E_\ell-E_{\ell'})^2+\eta^2} \\ &= \frac{1}{\omega}\sum_{\ell<\ell'}\langle u_\ell|\partial_\mu \mathrm{H}|u_{\ell'}\rangle\langle u_{\ell'}|\partial_\mu \mathrm{H}|u_\ell\rangle[f(E_\ell)-f(E_{\ell'})]\pi\delta(\omega+E_\ell-E_{\ell'}).\end{aligned} \tag{2-48}$$

Finally, using

$$\langle u_\ell|\partial_\mu \mathrm{H}|\ell'\rangle\langle u_{\ell'}|\partial_\mu \mathrm{H}|u_\ell\rangle = (E_\ell - E_{\ell'})\langle\partial_\mu u_\ell|u_{\ell'}\rangle(E_{\ell'}-E_\ell)\langle\partial_\mu u_{\ell'}|u_\ell\rangle \tag{2-49}$$

and since $\langle\partial_\mu u_{\ell'}|u_\ell\rangle = -\langle u_{\ell'}|\partial_\mu u_\ell\rangle$,

$$\langle u_\ell|\partial_\mu \mathrm{H}|u_{\ell'}\rangle\langle u_{\ell'}|\partial_\mu \mathrm{H}|u_\ell\rangle = (E_\ell - E_{\ell'})^2\langle\partial_\mu u_\ell|u_{\ell'}\rangle\langle u_{\ell'}|\partial_\mu u_\ell\rangle, \tag{2-50}$$

the expression above can be rewritten in other form. And also, putting back the lattice constant and $\hbar$ to male $\sigma_{\mu\mu}$ to have the right unit in D-dimension. In addition, the δ-function implies $\hbar\omega = E_\ell - E_{\ell'}$, then

$$\begin{aligned}\sigma_{\mu\mu}(\mathbf{k},\omega) &= \frac{\pi}{a^D\hbar\omega}\sum_{\ell<\ell'}\langle u_\ell|\partial_\mu \mathrm{H}|u_{\ell'}\rangle\langle u_{\ell'}|\partial_\mu \mathrm{H}|u_\ell\rangle[f(E_\ell)-f(E_{\ell'})]\delta(\omega+E_\ell-E_{\ell'}) \\ &= \frac{\pi e^2}{a^D}\hbar\omega g^d_{\mu\mu}(\mathbf{k},\omega),\end{aligned} \tag{2-51}$$

which introduces a quantum metric spectral function at finite temperature

$$\begin{aligned}g^d_{\mu\nu}(\mathbf{k},\omega) = \sum_{\ell<\ell'}\left\{\frac{1}{2}\langle\partial_\mu u_\ell|u_{\ell'}\rangle\langle u_{\ell'}|\partial_\nu u_\ell\rangle + (\mu\leftrightarrow\nu)\right\}\times \\ \times\left[f\left(\epsilon_{\ell\mathbf{k}}\right)-f\left(\epsilon_{\ell'\mathbf{k}}\right)\right]\delta\left(\omega+\frac{\epsilon_{\ell\mathbf{k}}}{\hbar}-\frac{\epsilon_{\ell'\mathbf{k}}}{\hbar}\right),\end{aligned} \tag{2-52}$$

where the quantities obtained this way will be called "dressed", indicated by the superscript d. This function have the physical interpretation of being a kind of "density of states" of the dressed quantum metric g^d, indicating the contribution given by each eigenstate for this quantity.

It is important to observe on the above expression, that the count over the states are different from the case at zero temperature, in section2.2. Now, the indices ℓ and ℓ' are used to indicate all the states of the system, under the condition that ℓ is always smaller than ℓ'. Following the same line of reasoning, the momentum integration of this function can give the conductivity of the whole sample measurable in space, implying on the integration of the quantum metric spectral function, obtaining

$$\begin{aligned}\sigma_{\mu\mu}(\omega) &= \int \frac{d^D\mathbf{k}}{(2\pi\hbar/a)^D}\sigma_{\mu\mu}(\mathbf{k},\omega) \\ &= \frac{\pi e^2}{\hbar^{D-1}}\omega \int \frac{d^D\mathbf{k}}{(2\pi)^D} g^d_{\mu\mu}(\mathbf{k},\omega) \equiv \frac{\pi e^2}{\hbar^{D-1}}\omega\, \mathrm{G}^d_{\mu\mu}(\omega),\end{aligned} \tag{2-53}$$

exposing this way, the relation between the conductivity of the sample and a finite temperature quantity named *fidelity number spectral function* $\mathrm{G}^d_{\mu\mu}(\omega)$.

Beside this, is now considered that the D-dimensional material is submitted to a oscillating electric field denoted now as $\mathrm{E}_\mu(\omega,t) = E_0\cos(\omega t)$, polarized in μ direction, where E_0 is its intensity. The current induced by this field is defined as

$$\begin{aligned}j_\mu(\omega,t) &= \sigma_{\mu\mu}(\omega)E_0\cos(\omega t) \\ &\equiv \frac{\pi e^2}{\hbar^{D-1}}\omega E_0\, \mathrm{G}^d_{\mu\mu}(\omega)\cos(\omega t)\end{aligned} \tag{2-54}$$

where such definition can be used now to calculate another experimental measurable quantity, the *optical absorption power* per unit cell also in function of the frequency ω

$$\begin{aligned}W_a(\omega) &= \langle j_\mu(\omega,t)E_\mu(\omega,t)\rangle_t = \frac{1}{2}\sigma_{\mu\mu}(\omega)E_0^2 \\ &= \frac{\pi e^2}{2\hbar^{D-1}}E_0^2\omega\, \mathrm{G}^d_{\mu\mu}(\omega),\end{aligned} \tag{2-55}$$

obtained by the time average $\langle\ldots\rangle_t$ of the multiplication of the field and its induced current. This expression suggests that the measure of the absorption power of the sample can be used to obtain the spectral function $\mathrm{G}^d_{\mu\mu}(\omega)$ in $\mu\mu$ direction.

Looking for a $2D$ system, the *incident power* of the light per unit area W_i is defined as

$$W_i = \frac{c\varepsilon_0 E_0^2}{2} \tag{2-56}$$

where c is the velocity of the light and ε_0 is the electric permissivity. Therefore, considering that the light is polarized in μ direction, the *opacity* of this $2D$ system can be defined as [32]

$$\mathcal{O}(\omega) = \frac{W_a(\omega)}{W_i} = 4\pi^2\alpha\omega\, \mathrm{G}^d_{\mu\mu}(\omega)|_{2D}, \tag{2-57}$$

where the term $\alpha = e^2/4\pi\varepsilon_0\hbar c$ is the fine structure constant, and the expression can be managed to define the spectral function of such opacity

$$\mathrm{G}^d_{\mu\mu}(\omega)|_{2D} = \frac{1}{4\pi\omega}\left[\frac{\mathcal{O}(\omega)}{\pi\alpha}\right], \tag{2-58}$$

leading to conclude that once the opacity is obtained, is possible to get the fidelity number spectral function through the simple relation above, which is basically this opacity in units of $\pi\alpha$ multiplied by a factor of $1/4\pi\omega$. Even that

this formulation has been recently applied in two-dimensional Dirac materials , such as graphene, is expected that it works broadly for two-dimensional systems.

Continuing in the $2D$ approach, the way to get the off-diagonal terms of the spectral function, referred to be $\mathrm{G}^d_{\mu\nu}(\omega) \to \mathrm{G}^d_{xy}(\omega)$, is consider a different polarization of the light [33], where now the field, current operator mentioned above are defined as

$$\begin{aligned} E_\pm &= E_0(\hat{x} \pm \hat{y}) \\ \hat{j}_\pm &= \hat{j}_x \pm \hat{j}_y \end{aligned} \tag{2-59}$$

which leads to a respective conductivity $\sigma_\pm(\mathbf{k}, \omega)$. Then, the off-diagonal components of the quantum metric spectral function can be obtained relating then as

$$\sigma_+(\mathbf{k}, \omega) - \sigma_-(\mathbf{k}, \omega) = \frac{4\pi e^2}{a^D} \hbar\omega g^d_{xy}(\mathbf{k}, \omega), \tag{2-60}$$

whose momentum integration shall connect G^d_{xy} with the current operator $\hat{j}_\pm$, which will be used to fisnd the difference of the absorption power

$$\begin{aligned} \Delta W_a(\omega) &= \langle j_+(\mathbf{k}, \omega) E_+(\mathbf{k}, \omega) - j_-(\mathbf{k}, \omega) E_-(\mathbf{k}, \omega) \rangle \\ &= \frac{2\pi e^2}{\hbar^{D-1}} E_0^2 \omega \, \mathrm{G}^d_{xy}(\omega). \end{aligned} \tag{2-61}$$

Making the same process done before, in which the absorption power was divided by the incident power, obtaining the difference between opacities with different direction of polarization can give the component of the spectral function

$$\mathrm{G}^d_{xy}(\omega)|_{2D} = \frac{1}{8\pi\omega} \left[\frac{\mathcal{O}_+(\omega) - \mathcal{O}_-(\omega)}{\pi\alpha} \right], \tag{2-62}$$

concluding then, that the measurement of the opacity of such $2D$ materials can give a complete information about its finite temperature fidelity spectral function, what suggests that results of experimental measurements are very potential means to obtain information about the topology of such materials.

Development of the finite temperature fidelity marker

Once the dressed fidelity spectral function was obtained through linear response theory, it is possible to use it to obtain the dressed fidelity number, which one is calculated considering the effect of temperature over the material. Then, doing a similar process which was done on eq.2-18,

$$\begin{aligned} \mathrm{G}^{\mathrm{d}}_{\mu\nu} &= \int_0^\infty G^d_{\mu\nu}(\omega) d\omega \\ &= \int \frac{d^D\mathbf{k}}{(2\pi)^D} \sum_{\ell<\ell'} \left[\frac{1}{2} \langle \partial_\mu u_\ell | u_{\ell'} \rangle \langle u_{\ell'} | \partial_\nu u_\ell \rangle + (\mu \leftrightarrow \nu) \right] \left[f(\epsilon_{\ell\mathbf{k}}) - f(\epsilon_{\ell'\mathbf{k}}) \right] \end{aligned} \tag{2-63}$$

where is possible to to see that the expression into brackets, which is similar to the last case, is being multiplied by the Fermi distributions of each energy state. It then follows that, the momentum integration can be splitted in intagrations over $\mathbf{k}$ and $\mathbf{k}'$,

$$\mathrm{G}^{\mathrm{d}}_{\mu\nu} = \frac{1}{\hbar^2}\int \frac{d^D\mathbf{k}}{(2\pi)^D}\sum_{\ell<\ell'}\times \\ \times\left[\frac{1}{2}\left\langle\psi_{\ell\mathbf{k}}|\hat{\mu}|\psi_{\ell'\mathbf{k}}\right\rangle\left\langle\psi_{\ell'\mathbf{k}}|\hat{\nu}|\psi_{\ell\mathbf{k}}\right\rangle + (\mu\leftrightarrow\nu)\right]\left[f\left(\epsilon_{\ell\mathbf{k}}\right) - f\left(\epsilon_{\ell'\mathbf{k}}\right)\right] \quad (2\text{-}64)$$

$$= \frac{\hbar^{D-2}}{a^D}\int \frac{d^D\mathbf{k}}{(2\pi\hbar/a)^D}\int \frac{d^D\mathbf{k}'}{(2\pi\hbar/a)^D}\sum_{\ell<\ell'}\times \\ \times\left[\frac{1}{2}\left\langle\psi_{\ell\mathbf{k}}|\hat{\mu}|\psi_{\ell'\mathbf{k}'}\right\rangle\left\langle\psi_{\ell'\mathbf{k}'}|\hat{\nu}|\psi_{\ell\mathbf{k}}\right\rangle + (\mu\leftrightarrow\nu)\right]\left[f\left(\varepsilon_{\ell\mathbf{k}}\right) - f\left(\varepsilon_{\ell'\mathbf{k}'}\right)\right].$$

The Bloch functions can now be replaced by the eigenstates $|E_\ell\rangle$ of the lattice model, obtained via diagonalization, as

$$\mathrm{G}^{\mathrm{d}}_{\mu\nu} = \frac{\hbar^{D-2}}{Na^D}\sum_{\ell<\ell'}\left[\frac{1}{2}\left\langle E_\ell|\hat{\mu}|E_{\ell'}\right\rangle\left\langle E_{\ell'}|\hat{\nu}|E_\ell\right\rangle + (\mu\leftrightarrow\nu)\right]\left[f\left(E_\ell\right) - f\left(E_{\ell'}\right)\right] \quad (2\text{-}65)$$

which can also be simplified through using the projectors representation to be expressed in real space. To write this expression this way, the relation between Bloch states and lattice eigenstates is used again to rewrite the states as was made in Eq. 2-23,

$$\begin{aligned}\int \frac{d^D\mathbf{k}}{(2\pi\hbar/a)^D}|\psi_{\ell\mathbf{k}}\rangle\langle\psi_{\ell\mathbf{k}}| &\to \sum_\ell |E_\ell\rangle\langle E_\ell| = \sum_\ell \mathrm{S}_\ell, \\ \int \frac{d^D\mathbf{k}}{(2\pi\hbar/a)^D}|\psi_{\ell\mathbf{k}}\rangle\langle\psi_{\ell\mathbf{k}}|f(\epsilon_{\ell\mathbf{k}}) &\to \sum_\ell |E_\ell\rangle\langle E_\ell|f(\epsilon_{\ell\mathbf{k}}) = \sum_\ell \mathrm{S}_\ell f(\epsilon_{\ell\mathbf{k}}),\end{aligned} \quad (2\text{-}66)$$

and can be seen here that $|\psi_{\ell\mathbf{k}}\rangle$ is the full Bloch state, which periodic part $|u_{\ell\mathbf{k}}\rangle$ satisfies $\langle\mathbf{r}|\psi_{\ell\mathbf{k}}\rangle = e^{i\mathbf{k}\cdot\mathbf{r}}\langle\mathbf{r}|u_{\ell\mathbf{k}}\rangle$. Observing that instead of using the letters P and Q, the letter S is used, since there is no strict distinction between valence and conduction band at finite temperature because both of them are partially filled. The subscript ℓ (or ℓ') is now the responsible to indicate if the projector corresponds to the higher $|E_\ell\rangle$ or lower energy level $|E_{\ell'}\rangle$, obtained by the diagonalization of the Hamiltonian H. Then, the expression for the dressed fidelity marker can get the form

$$\mathrm{G}^{\mathrm{d}}_{\mu\nu} = \frac{\hbar^{D-2}}{Na^D}\sum_{\ell<\ell'}\mathrm{Tr}\left[\frac{1}{2}\hat{\mu}S_{\ell'}\hat{\nu}S_\ell + (\mu\leftrightarrow\nu)\right]\left[f\left(E_\ell\right) - f\left(E_{\ell'}\right)\right]. \quad (2\text{-}67)$$

Here, is visible the similarity with the expression obtained for zero-temperature casse, in eq. 2-24. Will be possible to see further that, considering a zero

temperature regime for $\mathrm{G}^{d}_{\mu\nu}$, the function $f(E_\ell) = \theta(-E_\ell)$. Then, it becomes evident that under this condition the dressed fidelity number converges to the same value obtained by the zero temperature fidelity number derived before.

In order to formulate a finite temperature fidelity marker, the expression in eq. 2-67 can be rewritten in a even more compact form through using a specific matrix, which is also responsible to introduce the extra projector, as made in eq. 2-27,

$$\mathcal{M}_\mu = \sum_{\ell<\ell'} S_\ell \mu S_{\ell'} \sqrt{f_{\ell\ell'}}, \tag{2-68}$$

where $[f(E_\ell) - f(E_{\ell'})]$ was splitted into the multiplication of two square roots $\sqrt{f_{\ell\ell'}}$, and the term $f_{\ell\ell'}$ is just a short notation for $f(E_\ell) - f(E_{\ell'})$. Using this, is possible to derive the finite temperature fidelity marker

$$\mathrm{G}^{\mathrm{d}}_{\mu\nu}(\mathbf{r}) = \frac{\hbar^{D-2}}{2a^D} \mathrm{Re}\left\{ \langle \mathbf{r}| \left[\mathcal{M}_\mu \mathcal{M}^\dagger_\nu + \mathcal{M}_\nu \mathcal{M}^\dagger_\mu \right] |\mathbf{r}\rangle \right\}, \tag{2-69}$$

which spatial sum can recover the dressed fidelity number

$$\mathrm{G}^{d}_{\mu\nu} = \sum_{\mathbf{r}} \frac{\mathrm{G}^{d}_{\mu\nu},(\mathbf{r})}{N}, \tag{2-70}$$

because the existence of the properties $\sum_{\mathbf{r}} |\mathbf{r}\rangle\langle\mathbf{r}| = I$ and $\mathrm{S}_\ell \mathrm{S}_{\ell'} = \delta_{\ell\ell'} \mathrm{S}_{\ell'}$ and also agree with the zero temperature fidelity marker results in eq. 2-26 doing $\lim_{T\to 0} \mathrm{G}^{d}_{\mu\nu}(\mathbf{r}) = \mathrm{G}_{\mu\nu}(\mathbf{r})$.

To keep the pattern of the procedures made earlier in this chapter for the zero temperature case, a Fourier transform of the dressed quantum metric can also be done here as in eq. 2-29,

$$\tilde{g}^{d}_{\mu\nu}(\mathbf{R}') = \int \frac{d^D\mathbf{k}}{(2\pi)^D} e^{i\mathbf{k}\cdot\mathbf{R}'} \int_0^\infty g^{d}_{\mu\nu}(\mathbf{k},\omega) d\omega, \tag{2-71}$$

and this dressed Wannier state correlation function can derive a similar expression to eq. 2-33, but now for the finite temperature case,

$$\mathrm{G}^{\mathrm{d}}_{\mu\nu}(\mathbf{r}+\mathbf{R},\mathbf{r}) = \frac{\hbar^{D-2}}{2a^D} \mathrm{Re}\left\{ \langle \mathbf{r}+\mathbf{R}| \left[\mathcal{M}_\mu \mathcal{M}^\dagger_\nu + \mathcal{M}_\nu \mathcal{M}^\dagger_\mu \right] |\mathbf{r}\rangle \right\}, \tag{2-72}$$

which is also be obtained by the $(\mathbf{r}+\mathbf{R},\mathbf{r})$-th off-diagonal matrix components.

As the connection between the dressed fidelity spectral function and a optical absorption power was done before, it is relevant to develop here, a fidelity marker spectral function. It can be obtained through multiplying this dressed fidelity spectral function by a Dirac delta function $\delta(\omega + E_\ell - E_{\ell'})$, and can be expressed trhough using a frequency dependent matrix

$$\mathcal{M}_\mu(\omega) = \sum_{\ell<\ell'} S_\ell \mu S_{\ell'} \sqrt{f_{\ell\ell'}\, \delta(\omega + E_\ell - E_{\ell'})}. \tag{2-73}$$

In the simulations this δ function can be represented by a Lorentzian $\delta(x) =$

$\frac{\eta}{\pi(x^2+\eta^2)}$, with η being an arbitrary very small number. Then, the dressed spectral function is derived as

$$\mathrm{G}^{\mathrm{d}}_{\mu\nu}(\mathbf{r},\omega) = \frac{\hbar^{D-2}}{2a^D}\,\mathrm{Re}\left\{\langle\mathbf{r}|\left[\mathcal{M}_\mu(\omega)\mathcal{M}^\dagger_\nu(\omega)+\mathcal{M}_\nu(\omega)\mathcal{M}^\dagger_\mu(\omega)\right]|\mathbf{r}\rangle\right\}, \tag{2-74}$$

which spatial sum results in the spectral function linked to the absorption power in eq. 2-55,

$$\mathrm{G}^{d}_{\mu\nu}(\omega) = \sum_{\mathbf{r}} \frac{\mathrm{G}^{d}_{\mu\nu}(\mathbf{r},\omega)}{N}, \tag{2-75}$$

making room for development of the calculation of the local absorption power correspondent to the system unit cell at position $\mathbf{r}$

$$\mathrm{W}_{\mathrm{a}}(\mathbf{r},\omega) = \frac{\pi e^2}{2\hbar^{D-1}} E_0^2\omega\,\mathrm{G}^{\mathrm{d}}_{\mu\mu}(\mathbf{r},\omega). \tag{2-76}$$

And as usual, the off-diagonal components of $\mathrm{G}^{\mathrm{d}}_{\mu\nu}(\mathbf{r},\omega)$ contain relevant information. In this case, it gives the absorption power difference shown in eq. 2-61. Due to its link with the ability to absorb energy, is expected that thermal probes capable of detecting the heating effects generated by light at the atomic level, like scanning thermal microscopy, will be able to perform this task.

As could be seen, this chapter focused in show the path took in the development of the theory behind this work. Even commenting each one of the results obtained, is obvious the necessity of a visualization of its behavior. The next chapter is then all devoted to showing the figures got for the main results, and each figure shown there was very discussed and compared with other results in order to make a concise work.

3
Applications in one- and two-dimensional models

After presenting the theoretical framework in this work, the primary objective is to demonstrate its application through examples of models for Topological Insulators (TIs). The calculations of the quantities discussed in the previous chapter were first analyzed analytically in linear Dirac models. Later, numerical calculations were conducted to study the behavior in real space using various lattice models. By employing both approaches, the results obtained through the implementation of the theory are compared to observe their concordance. This comprehensive analysis allows us to gain a deeper understanding of the theory's applicability and its behavior in different scenarios. The combination of analytical and numerical investigations provides valuable insights into the behavior and properties of Topological Insulators and enhances our confidence in the theoretical framework's validity.

3.1
The Su-Schrieffer-Heeger model

In a way to introduce the present model and understand it well, it is important to comment a little of its origin. This way, is necessary to start introducing an important polymer. The polyacetylene (PA), which chemical formula is $(C_2H_2)_n$, is an organic polymer discovered in the 70's by Hideki Shirakawa, Alan Heeger, and Alan MacDiarmid. It is known to be the simplest linear conjugated polymer, whose molecular structure is basically a chain, with single and double bonds between the carbon atoms in alternate positions, as shown in figure 3.1.

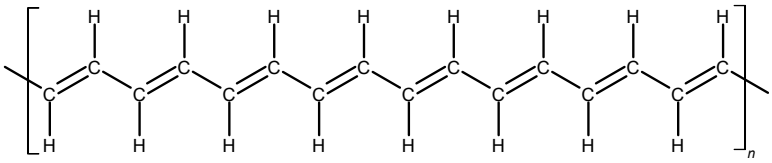

Figure 3.1: Representation of the chemical structure of *trans*-isomer of polyacetylene.

In 1979, W. P. Su, J. R. Schrieffer and A. J. Heeger presented pioneeringly a theoretical study involving to observe the occurrence of soliton formation in PA chains with *trans* configuration. Until current days, this work is used as basis to studies involving the well known Su-Schrieffer-Heeger (SSH) model. The SSH model[34] is a 1D toy model used to describe the PA chain. The chain

is composed by two sublattices, A and B, and its unit cell hosts one site of each sublattice [35]. In second quantization formalism it can be described by the Hamiltonian

$$H = \sum_i (t + \delta t) c_{Ai}^\dagger c_{Bi} + (t - \delta t) c_{Ai+1}^\dagger c_{Bi} + h.c. \tag{3-1}$$

where c_{Ai} and c_{Bi} and they hermitian conjugate are the annihilation and creation operators where is possible to see that they act on A and B sublattices of the model. The δt is the difference existent in the hopping between each basis and the atoms belonging to then, describing the presence of single and double bonds in the structure.

An important characteristic to be mention, is the effect the values assigned to δt has over the lattice. Different values for it results on different dimerization, which affects the material properties. The figure 3.2 schematizes types of patterns of the chain, where shows the case of setting $\delta t > 0$ (top chain) and $\delta t < 0$ (bottom chain), changing the organization of the sublattices.

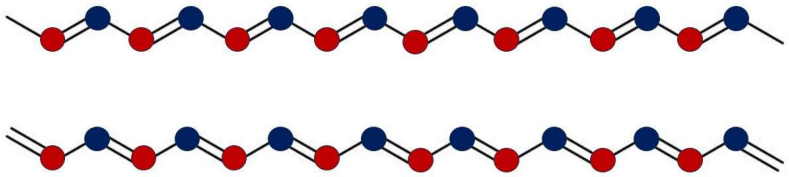

Figure 3.2: Schematic drawing of the two types of dimerization of the SSH model corresponding to values of $\delta t > 0$ (top) and $\delta t < 0$ (bottom).

In the present work, the numerical calculations for the SSH model were made only considering $\delta t < 0$. This suggests that the lattice simulated here was the bottom molecule representation on the figure above, which looking for its Hamiltonian in eq. 3-1, is possible to verify that it have a critical point in $\delta t = 0$. The numerical calculation of the local and non-local FM for this lattice model resulted in interesting results.

First, let's consider the local fidelity marker. The graph in Figure 3.3 illustrates the fidelity marker's profile over the real space, displaying the values of this quantity for each of the 100 simulated lattice unit cells. The calculations were performed with different values of δt, specifically $\delta t = -0.1$, $\delta t = -0.2$, and $\delta t = -0.3$, at both zero temperature ($K_B T = 0$) and non-zero temperature ($K_B T = 0.05$).

As expected, the fidelity marker profile exhibits constant values in the bulk, which increase as δt approaches zero and tend to diverge near the edges. It is noteworthy that the results for the finite temperature fidelity marker (represented by dashed lines) do not significantly differ from the zero temperature results (represented by solid lines). The only noticeable variation

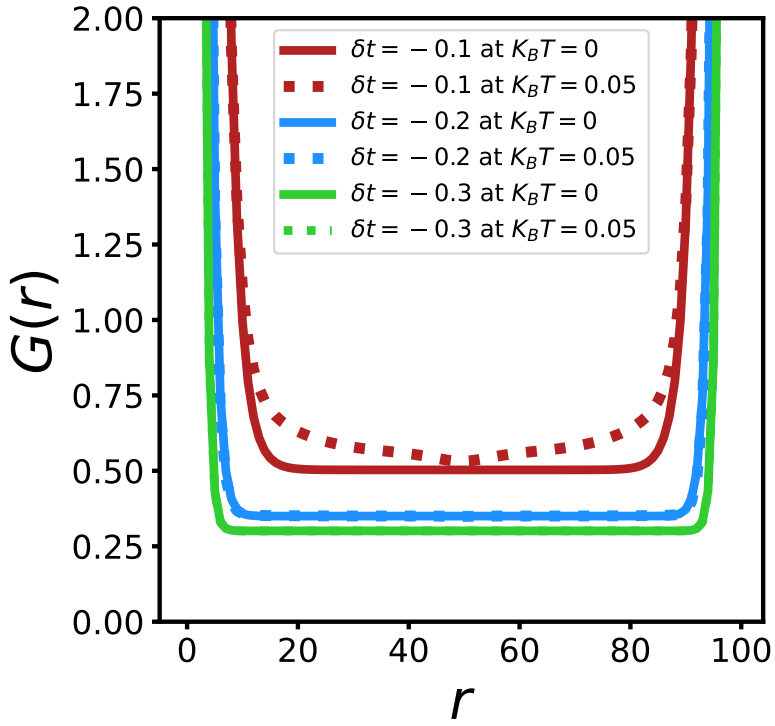

Figure 3.3: Numerical results of the fidelity marker at different values of tuning parameter δt, and at zero and a finite temperature. The value in the flat region in the large part of the sample agrees with the momentum integration of the quantum metric, indicating the validity of the marker.

occurs at higher temperatures. This behavior indicates the robustness of the fidelity number associated with the system, as it remains virtually unchanged at low temperatures and varies only under higher temperature conditions. This robustness of the fidelity number is observed in other examples that will be discussed later in this chapter. Such stability in the fidelity number reinforces the topological properties of the system and its insensitivity to thermal fluctuations.

The non-local fidelity marker, shown in figure 3.4, plotted for the same lattice with different δt displays an interesting pattern. As commented in the last chapter, the non-local marker provides the correlation over the system. The calculations were made for a chosen unit cell in the middle of the lattice, this way, the marker shows the correlation between the chosen unit cell and the entire lattice. Therefore, its real space profile provide a visualization of the correlation length for each δt, as long it approach the critical point at $\delta t = 0$, displaying the characteristic behavior of the quantum phase transition indicator. For the red graphic ($\delta t = -0.1$), the correlation length is long ranged as it shortens when the value of δt moves away from the critical point, as shown in the blue ($\delta t = -0.2$) graphic and subsequently even shorter in the

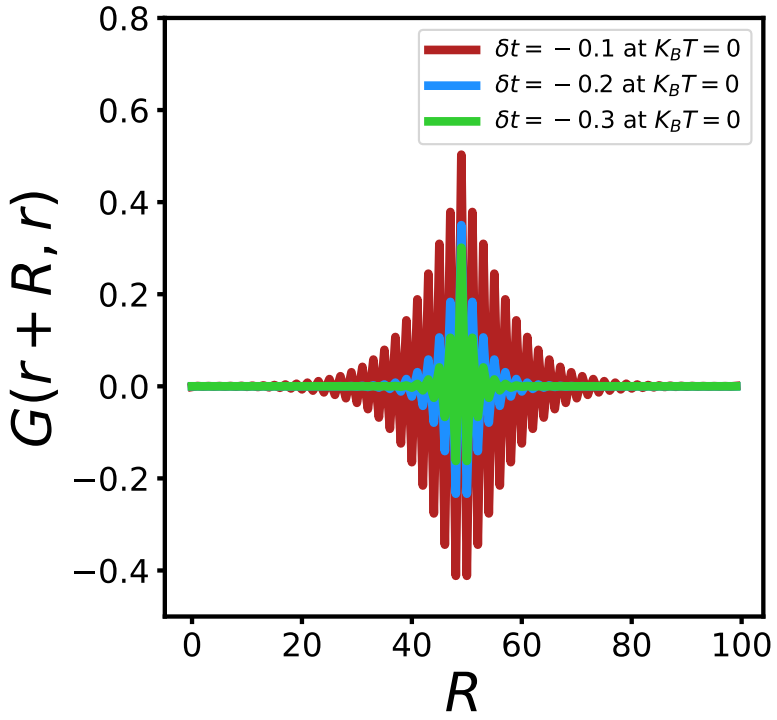

Figure 3.4: Numerical results of the nonlocal fidelity marker at several different values of δt. One sees that the nonlocal marker becomes more long ranged as the system approaches the critical point $\delta t = 0$.

green ($\delta t = -0.3$) graphic. This result agrees with what is expected, since the quantum metric in momentum space diverges like a peak as the system approaches the critical point, and hence its Fourier transform (the non-local marker) must become more long ranged.

In fact, these behavior of the local and non-local fidelity marker can be directly examine in momentum space, because the analytical form of the quantum metric can be easily obtained. Upon acting the following Fourier transform in the creation and annihilation operators, respectively, of the Hamiltonian in eq.3-1

$$c^{\dagger}_{Ai} = \sum_k e^{-i\mathbf{k}r_i} c^{\dagger}_{A\mathbf{k}}, \;\; c_{Ai} = \sum_k e^{i\mathbf{k}r_i} c_{A\mathbf{k}}, \tag{3-2}$$

it is possible to write it in function of momentum. Doing this for both A and B sublattices, the SSH Hamiltonian takes the form

$$H = \sum_k \left[(t+\delta t) + (t-\delta t)e^{-ik}\right] c^{\dagger}_{Ak} c_{Bk} + \left[(t+\delta t) + (t-\delta t)e^{ik}\right] c^{\dagger}_{Bk} c_{Ak}, \tag{3-3}$$

which can be splitted isolating the operators from the hopping term expressions, resulting in the matrix multiplication

$$
\begin{aligned}
H &= \sum_k \begin{pmatrix} c_{Ak}^\dagger & c_{Bk}^\dagger \end{pmatrix} \begin{pmatrix} 0 & (t+\delta t)+(t-\delta t)e^{-ik} \\ (t+\delta t)+(t-\delta t)e^{ik} & 0 \end{pmatrix} \begin{pmatrix} c_{Ak} \\ c_{Bk} \end{pmatrix} \\
&= \sum_k \begin{pmatrix} c_{Ak}^\dagger & c_{Bk}^\dagger \end{pmatrix} (\mathrm{d}\cdot\sigma) \begin{pmatrix} c_{Ak} \\ c_{Bk} \end{pmatrix},
\end{aligned} \tag{3-4}
$$

where σ are the Pauli matrices that are multiplied by the vector d, satisfying the Dirac Hamiltonian, whose components are

$$
\begin{aligned}
d_1 &= (t+\delta t)+(t-\delta t)\cos k, \\
d_2 &= (t-\delta t)\sin k, \\
d_3 &= 0.
\end{aligned} \tag{3-5}
$$

After putting the components shown in the eq.3-5 into the quantum metric formula for Dirac models presented in eq.3-7, its possible to obtain the quantum metric for the SSH model, which results of its momentum integration shows concordance with the numerical results for the fidelity marker presented above. The general formula for the quantum metric in a Dirac model is derived below.

For N-dimensional ($N \times N$) Dirac models, described by a Hamiltonian of the type

$$
H = \sum_{i=0}^{D} d_i \Gamma_i, \tag{3-6}
$$

where Γ_i are the Dirac matrices and d_i are the components of the vector d, which characterizes the momentum dependence of the Hamiltonian. It has been previously demonstrated that the fully antisymmetric valence Bloch state of a TI, as represented by equation 2-16 and described by momentum $\mathbf{k}$, yields the quantum metric given by [27]

$$
g_{\mu\nu}(\mathbf{k}) = \frac{N}{8d^2}\left\{\sum_{i=0}^{D} \partial_\mu d_i \partial_\nu d_i - \partial_\mu \mathrm{d}\partial_\nu \mathrm{d}\right\}, \tag{3-7}
$$

where $\mathrm{d} = \sqrt{\sum_{i=0}^{D} d_i^2}$. According to the theory behind Dirac models, this state exhibits a $N/2$-fold degeneracy, with valence-band states having an energy of $\epsilon_n = -\mathrm{d}$ and conduction-band states with energy $\epsilon_m = \mathrm{d}$. The next step involves utilizing this expression for the quantum metric to calculate its related quantities, where the model's homogeneity leads to the following expression:

$$
\mathrm{G}_{\mu\nu}^{d}(\omega) = \int \frac{d^D\mathbf{k}}{(2\pi)^D} g_{\mu\nu}^{d}(\mathbf{k},\omega)\left[f(\epsilon_n) - f(\epsilon_m)\right]\delta(\omega + \frac{\epsilon_n}{\hbar} - \frac{\epsilon_m}{\hbar}), \tag{3-8}
$$

which allows for the determination of both the fidelity number spectral function in eq.2-53 and the fidelity marker spectral function in eq. 2-74, since they are the same. The fidelity number can then be obtained either from a frequency integration of the fidelity number spectral function in Eq. 3-8, or from a

momentum integration of the quantum metric in Eq. 3-7. It was verified that, either way, one obtains a fidelity number that is consistent with the values in the flat region in Fig 3.3, indicating the validity of the numerical calculations of the fidelity marker made in this work.

3.2 2D Chern insulator

Lattice systems can exist where Bloch bands have a non-zero Chern number, denoting a topological property, even when there is no presence of magnetic field. In such instances, the insulator would be called a Chern insulator.

The 2D Chern insulator stands as one of the most pivotal and influential models in the realm of topological insulators. The first model of this kind, known as the Haldane model, was first introduced by F. D. M. Haldane in 1988 [36]. It describes a quantum Hall effect in a honeycomb lattice with broken time-reversal symmetry. The Haldane model is a paradigmatic example of a topological insulator, and it has gained immense importance in condensed matter physics due to its unique properties and behavior. As a two-dimensional system, the Chern insulator disrupts time-reversal symmetry, distinguishing it from conventional insulators. One of the defining features of the Chern insulator is the quantized Hall conductance that it exhibits. This quantization is described by the Chern number, a topological invariant that characterizes the topological properties of the system, as mentioned in chapter 2. The Chern number serves as a robust and fundamental measure of the topological nature of the 2D Chern insulator. This remarkable phenomenon has garnered significant attention and research interest, as it provides a concrete and experimentally observable manifestation of the topological nature of insulating materials.

When the Hall conductance of this model undergoes a sudden and discrete change from one value to another, it indicates a topological phase transition (TPT) in the system. In this context, the objective is to demonstrate how the fidelity marker can be employed to detect such a transition. This implies that the shift in quantized Hall conductance can be observed and measured through optical means.

In the present work, the concept of the 2D Chern insulator is applied here to a square lattice, as illustrated in Figure 3.5. The matrices in this case operate within a space composed of orbitals. A crucial aspect of this system is that the kinetic part of the Hamiltonian is characterized by an odd dependence on the momentum $\mathbf{k}$. The unique property of this interaction leads to intriguing

topological behavior, making the 2D Chern insulator a compelling platform for studying and understanding topological phenomena in condensed matter systems.

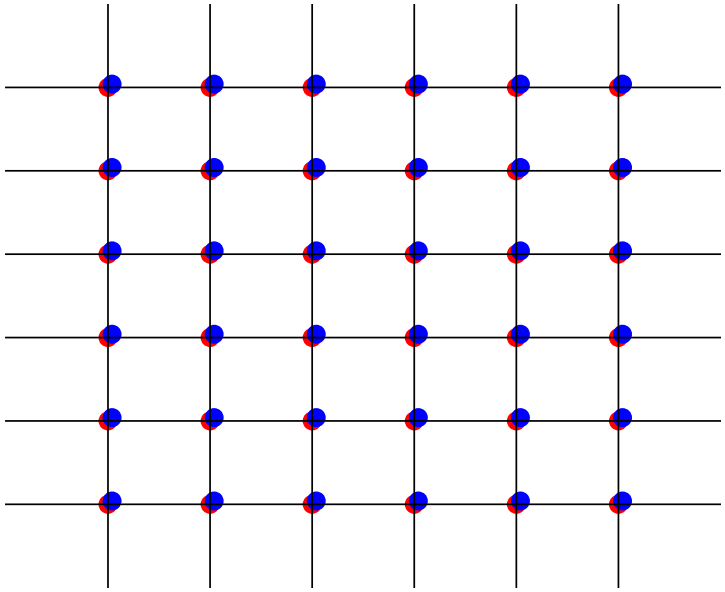

Figure 3.5: Pictorial representation of the simulated square lattice to obtain the numerical results of this work.

The fig. 3.5 serves as a schematic representation of the 2D Chern insulator, which was simulated to derive the numerical results for the local and non-local fidelity markers. The figure illustrates a 6×6 square lattice, with the sites represented by the intersection of black lines. Within the lattice, two circles, one red and one blue, are depicted superimposed on each other. These differently colored circles symbolize the two possible s- and p-orbitals that can be occupied within the model. Hence, the simulation of the model is based on the premise that the Chern insulator is described by the spinless basis $\psi = (c_{\mathbf{k}s}, c_{\mathbf{k}p})^T$ and by the following Hamiltonian expanded in terms of three Pauli matrices

$$\begin{aligned} H(\mathbf{k}) =& A \sin k_x \sigma^x + A \sin k_y \sigma^y \\ &+ (M + 4B - 2B \cos k_x - 2B \cos k_y)\, \sigma^z, \end{aligned} \tag{3-9}$$

which satisfy the Dirac Hamiltonian, with

$$\begin{aligned} d_1 &= A \sin k_x, \\ d_2 &= A \sin k_y, \\ d_3 &= M + 4B - 2B \cos k_x - 2B \cos k_y. \end{aligned} \tag{3-10}$$

Here, the parameters A and B are associated with the kinetic terms related to hopping, and $\{\sigma_x, \sigma_y, \sigma_z\}$ represent the Pauli matrices. The terms $k_\ell =$

$\{k_x, k_y, k_z\}$ account for the kinetic terms responsible for the usual linear band crossing, while the mass term M controls the system's topology.

To rewrite the Hamiltonian in real space, the Fourier transform acts on the spinless basis of electron creation and annihilation operators, $c^\dagger_{kI}$ and c_{kI}, as follows:

$$\begin{aligned}\sum_k \cos(k_\ell) c^\dagger_{kI} c_{kJ} &\to \frac{1}{2}\sum_i \left\{ c^\dagger_{iI} c_{(i+\ell)J} + c^\dagger_{(i+\ell)I} c_{iJ} \right\}, \\ \sum_k \sin(k_\ell) c^\dagger_{kI} c_{kJ} &\to \frac{1}{2}\sum_i \left\{ c^\dagger_{iI} c_{(i+\ell)I} + c^\dagger_{(i+\ell)I} c_{iJ} \right\},\end{aligned} \tag{3-11}$$

As a result of this Fourier transform, the operators with momentum $\mathbf{k}$ that act on orbitals $I = \{s, p\}$ are transformed into real space operators. These new operators are the ones used to construct the real space second quantized Hamiltonian defined on lattice sites i [37]

$$\begin{aligned}H = &\sum_i t \left\{ -i c^\dagger_{is} c_{(i+a)p} + i c^\dagger_{(i+a)s} c_{ip} + \text{ H.c. } \right\} \\ &+ \sum_i t \left\{ -c^\dagger_{is} c_{(i+b)p} + c^\dagger_{(i+b)s} c_{ip} + \text{ H.c. } \right\} \\ &+ \sum_{i\delta} t' \left\{ -c^\dagger_{is} c_{(i+\delta)s} + c^\dagger_{ip} c_{(i+\delta)p} + \text{ H.c.} \right\} \\ &+ \sum_i (M + 4t') \left\{ c^\dagger_{is} c_{is} - c^\dagger_{ip} c_{ip} \right\} - \sum_{il} \mu c^\dagger_{iI} c_{iI}.\end{aligned} \tag{3-12}$$

In this real space representation, the lattice constants for each direction of the plane are denoted as $\delta = a, b$. The hopping terms, $t = A/2$ and $t' = B$, act on the sites i, involving the two possible orbitals, I. It is important to note that the chemical potential μ, which appears at the end of the expression, will be considered zero in the subsequent simulations. The decision to ignore the chemical potential is due to its lack of influence on the topology of the system. Consequently, setting μ to zero simplifies the analysis without affecting the essential topological properties of the 2D Chern insulator.

Moreover, it is crucial to consider *periodic boundary conditions* in both directions for this real space representation. These boundary conditions are essential for studying the profile of the local and non-local fidelity markers for the 2D Chern insulator in a comprehensive manner. By employing periodic boundary conditions, the system behaves as if it were wrapped into a toroidal shape. This handling enables the study of properties that arise due to the system's topological nature, ignoring effects that occurs at the edges to look just to what happens in bulk of the system.

Numerical simulations were conducted on a 14×14 square lattice to study the intriguing behavior of a 2D Chern insulator and to reproduce the marker profiles presented in section 3.1, for the SSH model. The primary objective was

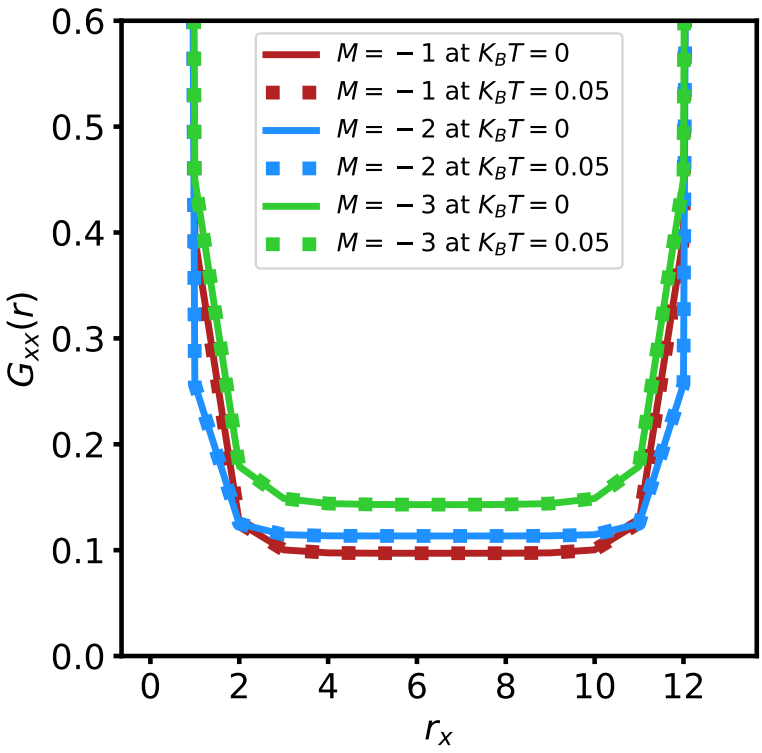

Figure 3.6: Numerical results for the local marker in the Chern insulator at several different parameters and temperatures. For the zero temperature data, the flat region in the center gives a value that agrees with the momentum integration of quantum metric in momentum space.

to develop a program capable of accurately diagonalizing the Hamiltonian in eq. 3-12 associated with the system, employing the *tight-binding* method. By obtaining the eigenvalues and eigenvectors through the diagonalization process, the markers could be effectively computed and analyzed.The resulting profile of the local fidelity marker, as depicted in Figure 3.6, visually illustrates the fidelity number's distribution across the real-space lattice on the x direction. This crucial data provides valuable insights into the system's quantum geometric properties. To ensure the robustness of the results and for comparative purposes, the simulations were repeated six times, each time varying the parameters. The investigation involved exploring the system under different mass terms, including $M = -1$ (red graphic), $M = -2$ (blue graphic), and $M = -3$ (green graphic), while also considering temperature conditions with $K_BT = 0$ and $K_BT = 0.05$. By studying the system's behavior under diverse temperature settings, it was possible to observe the effect of temperature on the marker values and assess the system's stability and consistency.

It is important to note that the behavior of the marker's profile presented here is the same as the one shown for the SSH model in the last section. Similarly, the marker exhibits a line of almost constant values in the center of

the graph that increases as the mass term change $M = -1 \rightarrow M = -2 \rightarrow M = -3$, and while approaching the edges, its values begin to increase until diverging at the boundary sites. The observed divergence in both models may appear to be a peculiar behavior, especially considering that the system has periodic boundary conditions. One would expect constant values throughout the graph, not just in the bulk region. However, this divergence occurs because the most straightforward way of assigning the position operator matrix does not respect the translational invariance of the system, a problem known for this kind of theory since the very first work of the Chern marker [18]. Nevertheless, the numerical results still reliable in the sense that for the region deep inside the bulk, one obtains a fidelity marker consistent with the fidelity numer calculated from the momentum integration of the quantum metric.

Since we are dealing with a 2D system, the marker can be obtained for two possible directions. This means that we can calculate $\mathrm{G}_{xx}(\mathbf{r})$, $\mathrm{G}_{yy}(\mathbf{r})$, and $\mathrm{G}_{xy}(\mathbf{r})$, as described in eq. 2-26 and eq. 2-69. However, in this work, we have only considered the values for the xx and yy directions. The marker parameterized in the xy direction does not offer as much useful information as the other cases since it is merely a superposition of them. As a result, it was not included in the analysis.

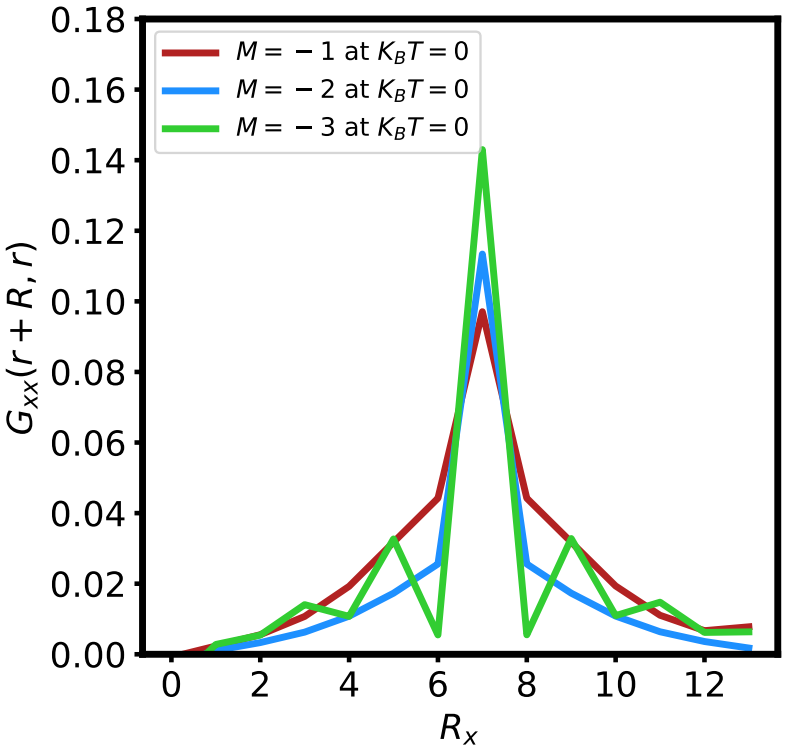

Figure 3.7: The nonlocal fidelity marker for the Chern insulator. One sees that the marker becomes more and more long ranged at the system approaches the critical point $M = 0$.

Continuing with the results obtained from the numerical calculations for the 2D Chern insulator, Figure 3.7 illustrates the profile of the non-local fidelity marker linked to this system. To obtain the non-local marker under zero temperature conditions ($K_BT = 0$), it was used the same mass term values applied in the results of Figure 3.6. This calculation involved applying eq. 2-33 to obtain the non-local marker profile. In practice, obtaining the profile of the non-local fidelity marker involves utilizing only the off-diagonal terms of the fidelity marker operator matrix corresponding to the arbitrarily selected site, while considering the two available orbitals. Consequently, when plotting a graph in the xx direction, one can observe the behavior of this marker for a site chosen near the center of the lattice. This selection of a site close to the middle of the lattice enables easy visualization and examination of the marker's properties.

It worth to mention that, through the Hamiltonian presented in eq. 3-9 is possible to see the values of M that corresponds to the critical points of the system. Then, these values of M were purposely chosen to enable the visualization of the markers approaching the critical points at $M = 0$ and $M = -4$. The result of the investigation shows that, the non local marker becomes more long ranged as it approaches the phase transition at $M = 0$, making possible to see how the correlation between the chosen site and its neighbors behaves.

A curious aspect of the non-local fidelity marker becomes apparent when the system approaches the critical point at $M = -4$. In the green graph representing the results for $M = -3$, one can observe an oscillating behavior that distinguishes it from the other cases. To understand this behavior, it is necessary to examine the regions $\mathbf{k} = \{k_x, k_y\}$ in the model's Brillouin zone corresponding to each critical point. The generic feature as the system approaches a TPT is that the quantum metric will peak and diverge at the corresponding gap-closing momentum.The critical point at $M = 0$ corresponds to a gap closing at $\mathbf{k} = \{0, 0\}$. Similarly, the critical point at $M = -4$ corresponds to gap closings at $\mathbf{k} = \{0, \pi\}$ and $\mathbf{k} = \{\pi, 0\}$. Thus, for the $M = -4$ critical point, the quantum metric also peaks at these two points. As a result, the non local fidelity marker as the Fourier transform of the quantum metric will oscillate in real space because of the peaks at $k = \{0, \pi\}$ and $k = \{\pi, 0\}$, consistent with our results shown in Fig 3.7. Then, this offer valuable insights into the system's critical behavior near this critical point.

This analysis not only reveals the robustness of the fidelity marker under varying temperature regimes but also helps to validate its effectiveness in detecting and characterizing quantum phase transitions in the 2D Chern

insulator. The numerical results provide compelling evidence of the marker's ability to capture the changes in quantized Hall conductance and open up exciting possibilities for optical detection and experimental investigations of topological and quantum geometrical phenomena in condensed matter systems.

4
Conclusion

In this work, we introduce the notion of fidelity number $\mathrm{G}_{\mu\nu}$, which is a quantity that is derived from the momentum integration of the quantum metric $g_{\mu\nu}$ of the fully antisymmetric valence-band state, and therefore quantifies the average distance between neighboring valence-band states within the Brillouin Zone torus. From the same formalism, we also introduce the nonlocal marker $\mathrm{G}_{\mu\nu}(\mathbf{r}+\mathbf{R},\mathbf{r})$ which demonstrates a decaying behavior with a correlation length ξ that becomes infinite near TPTs. The critical exponent $\nu = 1$ governing this divergence is universal for linear Dirac models in any dimension and symmetry class. Moreover, all quantities covered up to this point do not the effects of temperature, so they are said to be valid at zero temperature regime.

Through the application of linear-response theory, the concept of the fidelity number was extended to finite temperature, denoted as $\mathrm{G}^d_{\mu\nu}$. It was proposed that these quantities correspond to the optical absorption power W_a when subjected to linearly polarized light, which is directly related to the opacity $\mathcal{O}$ of 2D materials. The frequency dependence of this optical absorption power is described by a spectral function $\mathrm{G}^d_{\mu\nu}(\omega)$. Particularly in two-dimensional systems, this spectral function can be directly obtained from the frequency dependence of the opacity measured in units of the fine-structure constant. Furthermore, it was demonstrated that the fidelity number can be translated to real space as a local fidelity marker $\mathrm{G}^d_{\mu\nu}(\mathbf{r})$, defined on each unit cell. The corresponding spectral function $\mathrm{G}^d_{\mu\nu}(\mathbf{r},\omega)$ characterizes the local heating rate, which can be measured using atomic scale thermal probes. This measurement also provides insights into the gauge-invariant part of the spread of Wannier functions.

We further use TIs to elaborate the behavior of the aforementioned quantities, especially when they are approaching a critical point. It is found that when TIs are approaching a TPT, the quantum metric $g_{\mu\nu}$ displays singular behavior at the gap-closing HSPs. Consequently, this leads to a divergence in the fidelity number $\mathrm{G}^d_{\mu\nu}$ at the critical point in one and two dimensions. The corresponding spectral function $\mathrm{G}^d_{\mu\nu}(\omega)$ associated with the predicted fidelity number exhibits significant dependence on the system's dimension. Importantly, this behavior can be readily observed and measured experimentally in practical TIs through optical absorption techniques.

To better understand the behavior of these markers near critical points in realistic materials, prototype lattice models of TIs in one and two dimen-

sions were employed, providing a more accurate description. Although this study does not specifically cover calculations for a three-dimensional case, it is entirely feasible to conduct such analyses, which could yield intriguing outcomes. The results obtained from the research imply that these markers play a crucial role in characterizing the quantum geometry and quantum criticality across various topological materials, showcasing their wide-ranging significance in this context.

These characteristics of the fidelity number and marker hold significant implications for various applications. Firstly, the local nature of the marker allows it to be utilized in the study of how real-space inhomogeneities, such as impurities and grain boundaries, influence the material's quantum geometry. This provides valuable insights into the impact of local variations on the system's quantum properties. Secondly, the nonlocal fidelity marker, being the Fourier transform of the quantum metric, holds potential for detecting quantum phase transitions, as long as momentum remains a valid quantum number. This hypothesis is based on the understanding that the quantum metric $g_{\mu\nu}(\mathbf{k})$ essentially represents the fidelity susceptibility of the valence band state with respect to momentum $\mathbf{k}$. As a quantum phase transition is approached, the quantum metric is expected to diverge, resulting in a corresponding divergence in the decay length of the nonlocal marker. This suggests that the nonlocal fidelity marker could serve as a sensitive indicator of quantum phase transitions, even in cases where the transition is driven by weak interactions. These intriguing questions call for further investigations to shed light on the interplay between quantum geometry, quantum phase transitions, and the fidelity marker. Such studies should have the potential to offer new perspectives and a deeper understanding of fundamental quantum phenomena, advancing our knowledge of condensed matter systems and paving the way for innovative applications in quantum materials research, which await to be explored.

5
Bibliography

1 HASAN, M. Z.; KANE, C. L. Colloquium: Topological insulators. **Rev. Mod. Phys.**, American Physical Society, v. 82, p. 3045–3067, Nov 2010. Disponível em: <https://link.aps.org/doi/10.1103/RevModPhys.82.3045>.

2 QI, X. L.; ZHANG, S. C. Topological insulators and superconductors. **Reviews of Modern Physics**, v. 83, 10 2011. ISSN 00346861.

3 PROVOST, J. P.; VALLEE, G. **Mathematical Physics Riemannian Structure on Manifolds of Quantum States**. 1980. 289-301 p.

4 YOU, W. L.; LI, Y. W.; GU, S. J. Fidelity, dynamic structure factor, and susceptibility in critical phenomena. **Physical Review E - Statistical, Nonlinear, and Soft Matter Physics**, v. 76, 8 2007. ISSN 15393755.

5 ZANARDI, P.; GIORDA, P.; COZZINI, M. Information-theoretic differential geometry of quantum phase transitions. **Physical Review Letters**, v. 99, 9 2007. ISSN 00319007.

6 GU, S. J. et al. Fidelity susceptibility, scaling, and universality in quantum critical phenomena. **Physical Review B - Condensed Matter and Materials Physics**, v. 77, 6 2008. ISSN 10980121.

7 YANG, S. et al. Fidelity susceptibility and long-range correlation in the kitaev honeycomb model. **Physical Review A - Atomic, Molecular, and Optical Physics**, v. 78, 7 2008. ISSN 10502947.

8 ALBUQUERQUE, A. F. et al. Quantum critical scaling of fidelity susceptibility. **Physical Review B - Condensed Matter and Materials Physics**, v. 81, 2 2010. ISSN 10980121.

9 GU, S. J. Fidelity approach to quantum phase transitions. **International Journal of Modern Physics B**, v. 24, p. 4371–4458, 9 2010. ISSN 02179792.

10 CAROLLO, A.; VALENTI, D.; SPAGNOLO, B. **Geometry of quantum phase transitions**. [S.l.]: Elsevier B.V., 2020. 1-72 p.

11 SOUSA, M. S. M. de; CRUZ, A. L.; CHEN, W. Mapping quantum geometry and quantum phase transitions to real space by a fidelity marker. **Phys. Rev. B**, American Physical Society, v. 107, p. 205133, May 2023. Disponível em: <https://link.aps.org/doi/10.1103/PhysRevB.107.205133>.

12 SOUZA, I.; WILKENS, T.; MARTIN, R. M. **Polarization and localization in insulators: Generating function approach**.

13 MARZARI, N.; VANDERBILT, D. **Maximally localized generalized Wannier functions for composite energy bands**. 1997.

14 MARZARI, N. et al. Maximally localized wannier functions: Theory and applications. **Reviews of Modern Physics**, v. 84, p. 1419–1475, 10 2012. ISSN 00346861.

15 THOULESS, D. J. et al. Quantized hall conductance in a two-dimensional periodic potential. **Phys. Rev. Lett.**, American Physical Society, v. 49, p. 405–408, Aug 1982. Disponível em: <https://link.aps.org/doi/10.1103/PhysRevLett.49.405>.

16 PRODAN, E.; HUGHES, T. L.; BERNEVIG, B. A. Entanglement spectrum of a disordered topological chern insulator. **Physical Review Letters**, v. 105, 9 2010. ISSN 00319007.

17 PRODAN, E. **Erratum: Disordered topological insulators: A non-commutative geometry perspective (Journal of Physics A: Mathematical and Theoretical (2011) 44 (113001))**. 2011.

18 BIANCO, R.; RESTA, R. Mapping topological order in coordinate space. **Physical Review B - Condensed Matter and Materials Physics**, v. 84, 12 2011. ISSN 10980121.

19 CHEN, W.; GERSDORFF, G. von. Measurement of interaction-dressed berry curvature and quantum metric in solids by optical absorption. **SciPost Physics Core**, SciPost Foundation, v. 5, 7 2022. ISSN 26669366.

20 MAJUMDAR, A. **SCANNING THERMAL MICROSCOPY**. 1999. 505-85 p. Disponível em: <www.annualreviews.org>.

21 KITTEL, A. et al. Near-field heat transfer in a scanning thermal microscope. **Phys. Rev. Lett.**, American Physical Society, v. 95, p. 224301, Nov 2005. Disponível em: <https://link.aps.org/doi/10.1103/PhysRevLett.95.224301>.

22 GOMèS, S.; ASSY, A.; CHAPUIS, P. O. **Scanning thermal microscopy: A review**. [S.l.]: Wiley-VCH Verlag, 2015. 477-494 p.

23 ZHANG, Y. et al. **A Review on Principles and Applications of Scanning Thermal Microscopy (SThM)**. [S.l.]: Wiley-VCH Verlag, 2020.

24 VANDERBILT, D. **Berry Phases in Electronic Structure Theory**. [S.l.]: Cambridge University Press, 2018. ISBN 978-1-107-15765-1.

25 BERRY, M. V. Quantal phase factors accompanying adiabatic changes. **Proc. R. Soc. Land. A**, v. 392, 1984.

26 TAHERINEJAD, M.; GARRITY, K. F.; VANDERBILT, D. Wannier center sheets in topological insulators. **Physical Review B - Condensed Matter and Materials Physics**, American Physical Society, v. 89, 3 2014. ISSN 1550235X.

27 GERSDORFF, G. V.; CHEN, W. Measurement of topological order based on metric-curvature correspondence. **Physical Review B**, American Physical Society, v. 104, 11 2021. ISSN 24699969.

28 CHEN, W. et al. Correlation length, universality classes, and scaling laws associated with topological phase transitions. **Physical Review B**, American Physical Society, v. 95, 2 2017. ISSN 24699969.

29 ADVANCED Topological Insulators.

30 GRADHAND, M. et al. **First-principle calculations of the Berry curvature of Bloch states for charge and spin transport of electrons**. 2012.

31 MAHAN, G. D. **Many Particle Physics, Third Edition**. New York: Plenum, 2000.

32 NAIR, R. R. et al. Fine structure constant defines visual transparency of graphene. **Science**, v. 320, p. 1308, 6 2008. ISSN 00368075.

33 OZAWA, T.; GOLDMAN, N. Extracting the quantum metric tensor through periodic driving. **Physical Review B**, American Physical Society, v. 97, 5 2018. ISSN 24699969.

34 SU, W. P.; SCHRIEFFER, J. R.; HEEGER, A. J. **Solitons in Polyaeetylene**.

35 ASBÓTH, J.; OROSZLÁNY, L.; PÁLYI, A. **A Short Course on Topological Insulators: Band Structure and Edge States in One and Two Dimensions**. Springer International Publishing, 2016. (Lecture Notes in Physics). ISBN 9783319256078. Disponível em: <https://link.springer.com/book/10.1007/978-3-319-25607-8>.

36 HALDANE, F. D. M. Model for a quantum hall effect without landau levels: Condensed-matter realization of the "parity anomaly". **Phys. Rev. Lett.**, American Physical Society, v. 61, p. 2015–2018, Oct 1988. Disponível em: <https://link.aps.org/doi/10.1103/PhysRevLett.61.2015>.

37 CHEN, W. Absence of equilibrium edge currents in theoretical models of topological insulators. **Physical Review B**, American Physical Society, v. 101, 5 2020. ISSN 24699969.